Environment International 210 (2026) 110193

Contents lists available at ScienceDirect

Environment International

journal homepage: www.elsevier.com/locate/envint

Full length article

BeefPOP: a physiologically based toxicokinetic model describing the fate of polychlorinated biphenyls in growing beef cattle

Audrey Tiercin [a], John Albechaalany [a,b], Charlotte Driesen [a,c], Philippe Schmidely [b], Isabelle Ortigues-Marty [d], Markus Zennegg [c], Daniel Sauvant [b,1], Christelle Loncke [b], Sylvain Lerch [a,*]

[a] Ruminant Nutrition and Emissions, Agroscope, 1725 Posieux, Switzerland
[b] Université Paris-Saclay, INRAE, AgroParisTech, UMR Modélisation Systémique Appliquée aux Ruminants, 91120 Palaiseau, France
[c] Swiss Federal Laboratories for Materials Science and Technology Empa, Analytical Center, 8600 Dübendorf, Switzerland
[d] Université Clermont Auvergne, INRAE, Vetagro Sup, UMR Herbivores, 63122 Saint-Genès-Champanelle, France

ARTICLE INFO

Keywords:
Lipophilic contaminants
Food safety
Mechanistic model
Ruminant physiology
Adipose tissue
Toxicokinetic modeling

ABSTRACT

Polychlorinated biphenyls (PCBs) are persistent organic pollutants that bioaccumulate in livestock and threaten food safety. Understanding PCB kinetics in farm animals is essential for effective risk management. This study introduces BeefPOP, a mechanistic model that couples fugacity and physiologically based toxicokinetic concepts with animal feeding and physiology to simulate PCB kinetics in growing cattle. The model was optimized and evaluated using data from a toxicokinetic experiment involving Simmental cattle under controlled PCB exposure. BeefPOP demonstrated satisfactory predictive performance for adipose tissue PCB concentrations, with good accuracy (deviations below 1.4-fold of the biological observations and mean absolute percentage errors below 20%), and adequacy ($R^2 > 0.79$). Predictions for muscle and liver were slightly less satisfactory. Eighteen prospective scenarios were simulated, considering two cattle categories (Angus crossed Hereford steers and Charolais bulls), three growth itineraries (slow, fast, and compensatory growth), and three sources of PCB exposure (wall paint, contaminated feedstuff, and soil). Prospective simulations showed that PCB concentrations in adipose tissue were mostly influenced by growth rate, followed by cattle category and source of exposure. The highest bioconcentration factor was found in slow-growing Charolais bulls under wall paint exposure. Fast-growing early maturing cattle (i.e., Angus crossed Hereford steers) diluted PCBs more effectively due to shorter raising periods and higher lipid accretion. Such use of the model underscores the complex interplay between contaminant properties, growth physiology, and farming practices on PCB toxicokinetics. BeefPOP can support food safety risk management by predicting the fate of lipophilic contaminants in growing cattle under diverse farming scenarios.

Abbreviations: α, short phase decay constant; β, long phase decay constant; ADME, absorption, distribution, metabolism, excretion; AE, assimilation efficiency; AhR, aryl hydrocarbon receptor; AR, absorption rate; BCF, bioconcentration factor; C_b, bias correction factor; CCC, concordance correlation coefficient; CG, compensatory growth; CTL, control treatment; DIM, day in milk; DEC, depurated treatment; dl-PCB, dioxin-like-PCB; DM, dry matter; DMI, dry matter intake; EB, empty body; ECT, error proportion due to central tendency; ED, error proportion due to disturbance; ER, error proportion due to regression; EXP, exposed treatment; FG, fast growth; k_{met}, first-order metabolism rate constant; K_{ow}, partition coefficient between octanol and water; LBW, live body weight; LOD, limit of detection; MAPE, mean absolute percentage error; MB, mean bias; ME, metabolizable energy; ML, maximum level; MRT, mean retention time; ndl-PCB, non-dioxin-like-PCB; PBTK, physiologically based toxicokinetic model; PCDD/Fs, polychlorinated dibenzo-*p*-dioxins and dibenzofurans; PCBs, polychlorinated biphenyls; P_i, partition coefficient; POP, persistent organic pollutant; R^2, determination coefficient; RMSE, root mean square error; RRMSE, relative root mean square error; SG, slow growth; $t_{1/2}$, depuration half-life; WHO-TEQ, World Health Organization toxic equivalent of 2005.

* Corresponding author at: Ruminant Nutrition and Emissions, Agroscope, Route de la Tioleyre 4, 1725 Posieux, Switzerland.
E-mail address: sylvain.lerch@agroscope.admin.ch (S. Lerch).

[1] Author deceased.

https://doi.org/10.1016/j.envint.2026.110193
Received 24 November 2025; Received in revised form 7 March 2026; Accepted 9 March 2026
Available online 12 March 2026

1. Introduction

Polychlorinated biphenyls (PCBs) are synthetic chlorinated hydrocarbons classified as persistent organic pollutants (POPs) by the Stockholm Convention (Fiedler et al., 2019). Due to their chemical stability, thermal resistance, and insulating properties, PCBs were widely used in industrial products, such as electrical transformers, capacitors, paints, sealants, and lubricants (Erickson and Kaley, 2011). However, their high lipophilicity, persistence, and adverse effects on the environment and human health have led to restrictions and regulatory bans in many countries since the 1970s (Malisch and Kotz, 2014). Despite these measures, PCBs continue to pose significant risks due to unintentional release into the environment, including as byproducts of other chlorinated chemical productions, as well as their persistence (Hoogenboom et al., 2015; Weber et al., 2018a). According to their chlorination degree, substitution pattern and toxicological mode of action, PCBs are divided into two groups: 12 dioxin-like PCB congeners (dl-PCBs) and 197 non-dioxin-like PCB congeners (ndl-PCBs). Among ndl-PCBs, six congeners (28, 52, 101, 138, 153, 180) are monitored as indicators due to their high abundance, representing a large fraction of all PCBs (Hoogenboom et al., 2015). The dl-PCBs exhibit toxicological effects similar to that of polychlorinated dibenzo-*p*-dioxins and dibenzofurans (PCDD/Fs). Both are responsible of the activation of the aryl hydrocarbon receptor (AhR), which regulates genes involved in metabolism, endocrine function and organ homeostasis (Giesy and Kannan, 1998; EFSA, 2018). The ndl-PCBs do not activate AhR but can affect health through neurotoxic effects (Giesy and Kannan, 1998). The lipophilic nature of PCBs promotes their accumulation in animal fat tissues, causing chronic dietary exposure in humans through the consumption of foods of animal origin. In Europe, around 90% of total human exposure to PCBs and PCDD/Fs originates from animal-derived food, with dairy products and beef meat contributing significantly (EFSA, 2018; Weber et al., 2018b). Despite regulations on PCB levels in feed (EU regulation No 277/2012), several incidents of PCB contamination of farm animals and their food products have occurred in recent decades. These events originated from various exposure routes to PCBs, including diffuse environmental sources such as ingestion of contaminated soil, punctual sources such as contaminated barn materials, and the accidental or fraudulent incorporation of contaminated ingredients into animal feed (Weber et al., 2018a; Hoogenboom et al., 2020; Pajurek et al., 2022). Such incidents have led to serious economic and social consequences, including the disposal of contaminated herds and food products, disruptions of the agri-food sector, increased public concern, and social distress among affected farmers (Zennegg, 2018).

The effective management of risks posed by on-farm contaminants requires robust tools to accurately predict their fate within farm animals. Traditional empirical approaches based on animal toxicokinetic experiments have provided insights into PCB accumulation and depuration in animal tissues (Amutova et al., 2021; Krause et al., 2023). Findings from these approaches have allowed the computation of accumulation factors (i.e., bioconcentration, or biotransfer factors, and transfer rates) or depuration rates (half-lives). Nonetheless, such empirical factors are usually specific to the original experimental conditions (McLachlan, 1993) and are difficult to extrapolate to other husbandry scenarios. To address these limitations, compartmental and dynamic models have emerged as promising approaches for simulating lipophilic contaminant toxicokinetics in livestock (Moenning et al., 2023a; Mi and Lin, 2025). These models involve a comprehensive understanding of toxicokinetic processes—that is, the absorption, distribution, metabolism, and excretion (ADME) of contaminants—and their dependency on different nutritive and physiological stages of the animal along its lifespan.

Among the dynamic models for lipophilic contaminants developed for dairy cows (*e.g.*, Rosenbaum et al., 2009; Moenning et al., 2023b; Lerch et al., 2025), only a few address beef husbandry, particularly the case of growing and fattening cattle. MacLachlan and Bhula (2009) developed a mono-compartmental model representing lipophilic contaminant kinetics through basic absorption and elimination fluxes while considering the growth dynamic of cattle. However, the model's simplicity limits its capacity to distinguish tissue-specific kinetics or to dissociate metabolic from fecal excretion routes of elimination. Recently, Bogdal et al. (2017), Moenning et al. (2023c), and Minnema et al. (2025) adapted the initial cow model proposed by Derks et al. (1994) to integrate calf growth in the simulation of PCBs and PCDD/Fs contamination in suckler husbandry systems. Nonetheless, these models focused only on suckler cows and calves without any specific development for growing cattle after weaning. In these models, the growth dynamic is represented as a fixed trajectory, limiting their extrapolation to represent different production systems (Moenning et al., 2023a; Mi and Lin, 2025), although these factors are known to influence PCB and PCDD/Fs bioaccumulation and body distribution in growing cattle (Driesen et al., 2021; 2022b).

Indeed, among pre-existing models for lipophilic contaminant in growing cattle, none explicitly accounts for the feeding and physiological changes associated with various animal categories (sex and breed), diets, growth, and fattening itineraries in cattle intended for beef meat production. In addition, currently available models integrate PCB and PCDD/F absorption and fecal excretion processes as fixed parameters (Bogdal et al., 2017; Moenning et al., 2023c; Minnema et al., 2025) without any mechanistic description of intestinal transit and absorption to blood. This limitation prevents representing the effects of diet composition and PCB degree of lipophilicity on toxicokinetics. By contrast, McLachlan (1994) and more recently Lerch et al. (2025) applied the fugacity concept in lactating cows and accounted for lipophilic contaminant properties and digesta lipid content to represent the passive diffusion of contaminants across the intestinal barrier.

The aims of the present study are twofold. We (i) develop, optimize, and evaluate the predictive capabilities of a mechanistic model combining fugacity and physiologically based toxicokinetic (PBTK) concepts with a fine description of feeding and growth physiology to describe the toxicokinetic of individual congeners of dl-PCBs and indicator ndl-PCBs in growing beef cattle from birth to mature body weight (BW). We then (ii) apply this model to simulate various contamination scenarios, incorporating diverse PCB exposure sources and farming systems (cattle category and feeding intensity) for target risk assessment. By predicting PCB concentrations in tissues over time, such a model may support risk management decisions, including the estimation of withdrawal periods and timing of slaughter to ensure compliance with maximum levels (ML).

2. Materials and methods

2.1. Rationale and overview of the BeefPOP model

The BeefPOP model describes the fate of single congeners of lipophilic contaminants in growing beef cattle, and was optimized and evaluated for dl-PCBs and ndl-PCBs. In a mechanistic and generic approach, its design captures the physiological dynamics associated with growth, including BW gain, changes in tissue composition, various feed intakes, and digestibility. It further accounts for differences across cattle categories, such as early-maturing or late-maturing breeds and their respective feed intakes, growth rates, and body compositions. Combining a generic model of the mechanistic description of ADME of lipophilic contaminants with a detailed and flexible representation of feeding and growth physiology allows for a case-by-case exploration of the complex interplay between PCB properties, feeding strategies, and animal sex and breed on toxicokinetics. Ultimately, the purpose of this model is to serve as a decision-support tool for evaluating the fate of PCBs under realistic on-farm exposure scenarios in beef production systems.

2.1.1. Model concept and structure

The mechanistic model "BeefPOP" integrates both fugacity and PBTK

concepts to simulate the fate of lipophilic contaminants in growing beef cattle. The general framework is adapted from the PBTK model "RuMoPOP" developed by Lerch et al. (2025), which describes the transfer of lipophilic contaminants in lactating cows. A conceptual diagram of the BeefPOP model is presented in Fig. 1. The model consists of three interconnected sub-models. The first sub-model simulates the ADME of lipophilic contaminants in a mechanistic way, with further optimization for the 18 single PCB congeners regulated in feed (EU regulation No 277/2012) and food (EU regulation No 1259/2011). The second sub-model captures feed intake and lipid digestion based on equations from the INRA feeding system (INRA, 2018). The third sub-model represents the physiological processes involved in the growth of young cattle extracted from the mechanistic and teleonomic beef growth model of INRA "MecSiC" (Hoch and Agabriel, 2004a,b; Garcia et al., 2008).

2.1.2. ADME sub-model

The ADME sub-model (Fig. 1, black box) describes the fate of single PCB congeners in growing cattle. Table 1 lists the parameters and variables involved in the ADME processes of PCBs. It integrates mechanistic formalisms from fugacity (McLachlan, 1994; Mackay, 2001; Lerch et al., 2025) and PBTK models of lipophilic contaminants (MacLachlan, 2009) to capture the dynamic of PCB transfer throughout the cattle's organism. After oral ingestion, through specific or cumulative routes of exposure (i.e., solid feeds, milk, barn materials, or soil intakes), PCBs flow from the *Feed* to the *Rumen* and later the *Intestine* contents, where they are excreted via *Feces* or absorbed into *Blood*. From the *Blood*, PCBs are distributed to the *Liver* and *Perfused Adipose Tissues*, traveling further into *Deep Adipose Tissues*, *Muscles*, and *Others* compartments. Additionally, PCBs may return from the *Blood* to the *Intestines* by the non-biliary route and undergo reabsorption or excretion as *Feces*. Another route of elimination involves metabolic clearance that takes place in the *Liver* compartment. The transfer of PCBs involves three types of fluxes: advection, diffusion, or degradation.

Advective fluxes (indicated by red arrows in Fig. 1) describe the unidirectional transfer of the contaminant between compartments through a medium (i.e., digesta or blood), and are described according to the following equation:

$$Adv.Flow\ PCB_{i\to j}\ \left(ng.d^{-1}\right) = Q_{i\to j} \times \frac{A_i}{M_i}\left[\times \frac{1}{P_i}\right] \quad (1)$$

where $Q_{i\to j}$ is the flow of blood perfusion or digesta transit from compartment i to j (kg.d^{-1}), A_i is the amount of PCB in compartment i (ng), M_i is the mass of compartment i (kg), and P_i is the partition coefficient defined as the ratio of tissue i to blood contaminant concentration at equilibrium (unitless, only used for flows returning back from body tissue compartments to blood). Partition coefficients (P_i) are defined as the tissue i-to-blood lipid concentration ratios, assuming PCBs are diluted exclusively and homogeneously into lipids due to their high lipophilicity.

Diffusive fluxes (represented by orange arrow in Fig. 1) describe the passive bidirectional transfer of PCBs at the interface between the *Intestine* and *Blood* or *Perfused* and *Deep adipose tissue* compartments along the PCB concentration gradient (Mackay, 2001). For each interface, diffusion occurs sequentially across water and lipid layers, reflecting physiological interfaces of the intestinal microvilli and enterocyte membrane, or the adipocyte cytosol and membrane, respectively (Kelly et al., 2004; Lerch et al., 2025), according to the following equation:

$$Diff.Flow\ PCB_{i\to j}\ \left(ng.d^{-1}\right) = \frac{\frac{A_i}{V_{Lip_i}}}{\frac{K_{ow}}{Q_{Wat_{i/j}}} + \frac{1}{Q_{Lip_{i/j}}}} \quad (2)$$

where PCB concentration in compartment i equals the ratio of A_i, that is the amount of PCB in compartment i (ng), to V_{Lipi}, that is the mass of lipids in compartment i (kg lipids), K_{ow} is the PCB partition coefficient between octanol and water to convert a lipid- to a water-based concentration (unitless), and $Q_{Wati/j}$ and $Q_{Lipi/j}$ are the diffusive parameters across the water and lipid phases at the interface between compartments i and j, respectively (kg.d^{-1}). Details of the advective and diffusive flux calculations are provided in Supplementary Information S1.

Finally, the degradation of PCBs through metabolism is assumed to

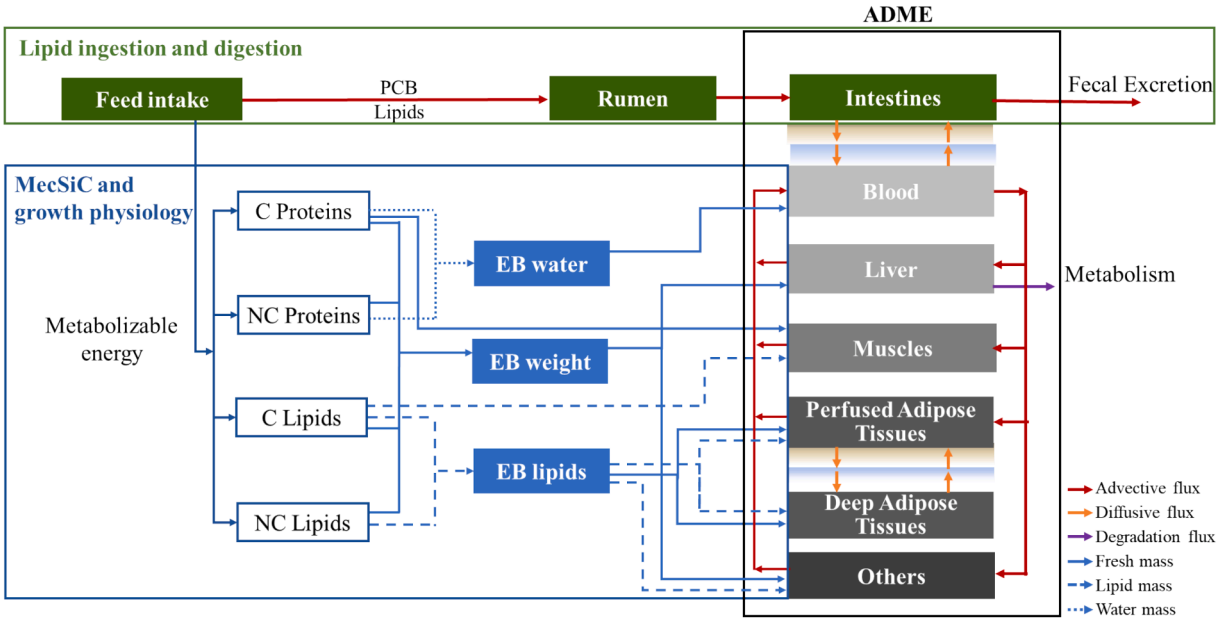

Fig. 1. Conceptual diagram of the physiologically based toxicokinetic model BeefPOP for non-dioxin-like polychlorinated biphenyl (ndl-PCB) and dioxin-like polychlorinated biphenyl (dl-PCB) in growing beef cattle. The green box represents the sub-model describing the feed intake, digestion, and absorption of lipids (INRA et al., 2018). The blue box represents the beef growth "MecSiC" sub-model (Hoch and Agabriel, 2004a,b), in which metabolizable energy intake is allocated for the syntheses of proteins and lipids in the carcass (C Proteins and C Lipids, respectively), and the non-carcass (NC Proteins and NC Lipids) compartments. The intake is subsequently allocated to empty body (EB) weight, EB water, and EB lipids, allowing further allocation of fresh and lipid masses across the different compartments of the sub-model describing the absorption, distribution, metabolism, and excretion (ADME) of PCBs (black box).

Table 1
Main parameters and variables of the absorption, distribution, metabolism, and excretion (ADME) of lipophilic contaminant and the physiological (ingestion, digestion, and growth) sub-model for growing cattle.

Item	Acronym	Unit	Description
Advection[a]			
Intake and fecal excretion			
	DMI[b]	kg.day^{-1}	Intake dry matter content
	$Q_{feed \rightarrow rumen}$[b]	kg lipids.day^{-1}	Lipids transit from the feed to the rumen
	$Q_{rumen \rightarrow intestine}$[b]	kg lipids.day^{-1}	Lipids transit from the rumen to the intestine
	$Q_{intestine \rightarrow feces}$[b]	kg lipids.day^{-1}	Fecal lipid excretion
Blood − tissue distribution			
	$Q_{blood\ /\ tissue\ i}$	kg.day^{-1}	Blood perfusion to the tissue i[c]
	Ai	ng	Amount of contaminant in tissue i[c]
	Mi	kg	Mass of the tissue i[c]
	Pi	unitless	Partition coefficient between blood and tissue i[c]
Diffusion[a]			
Contaminant lipophilicity			
	K_{ow}	unitless	Partition coefficient between octanol and water
Absorption and non-biliary excretion			
	$Q_{wat\_digestive\ contents/blood}$	kg.day^{-1}	Diffusive parameter across the water layer at the intestine/blood interface
	$Q_{lip\_digestive\ content/blood}$	kg.day^{-1}	Diffusive parameter across the lipid layer at the intestine/blood interface
Perfused-deep adipose tissues distribution			
	$Q_{wat\_perfused\ /\ deep\ adipose}$	kg.day^{-1}	Diffusive parameter across the water layer at the perfused/deep adipose tissues interface
	$Q_{lip\_perfused\ /\ deep\ adipose}$	kg.day^{-1}	Diffusive parameter across the lipid layer at the perfused/deep adipose tissues interface
Degradation[a]			
Hepatic clearance			
	k_{met}	day^{-1}	Metabolic first-order clearance rate in the liver
Physiological traits			
Solid feed lipid ingestion and digestion			
	IC[b]	kg.day^{-1}	Intake capacity
	Lipid intake[b]	g.day^{-1}	Intake lipid content
	DMI[b]	kg.day^{-1}	Intake dry matter content
	Lip Feed	g	Quantity of lipids from solid feed intake in the *Feed* compartment
	Lip $_{Feed \rightarrow Rumen}$[b]	g.day^{-1}	Transfer of lipids from *Feed* to *Rumen* compartment
	Lip Rumen	g	Quantity of lipids in the *Rumen* compartment
	Lip $_{Rumen \rightarrow Intestine}$[b]	g.day^{-1}	Transfer of lipids from *Rumen* to *Intestine* compartment
	Lip Intestine	g	Quantity of lipids in the *Intestine* compartment
	Lip $_{Intestine \rightarrow absorbed}$[b]	g.day^{-1}	Lipids absorbed in the *Intestine* compartment
	Lip $_{Intestine \rightarrow Feces}$[b]	g.day^{-1}	Lipids excreted in the feces
Growth			
	MEI	MJ.day^{-1}	Metabolizable Energy Intake
	Lip C[d]	kg	Lipid mass in the carcass
	Lip NC[d]	kg	Lipid mass in the non-carcass
	Prot C[d]	kg	Protein mass in the carcass
	Prot NC[d]	kg	Protein mass in the non-carcass
	BW[b]	kg	Live body weight
	EBW[b]	kg	Empty body weight
	Carcass mass[b]	kg	Carcass mass
	Lip EB[b]	kg	Empty body lipid mass
	Wat EB[b]	kg	Empty body water mass
	Prot EB[b]	kg	Empty body protein mass
	Mass i[b]	kg	Total fresh mass of the body compartment i[e]
	Lip i[b]	kg	Lipid mass of the body compartment i[e]

[a] Equations to determine the fluxes are described in the main text.
[b] Additional equations for parameter estimation are provided in Supplementary Information S2–S3.
[c] Tissue i refers to perfused adipose tissue, muscle, liver, or others.
[d] Lip C, Lip NC, Prot C, and Prot NC are calculated as the difference between lipid (Lip) or protein (Prot) synthesis and degradation in the carcass (C) and non-carcass (NC) compartments. Synthesis and degradation rates are estimated based on the maximum protein and lipid masses associated with the animal's maturity, according to the growth model of Hoch and Agabriel (2004a,b).
[e] Body compartment i refers to blood, perfused adipose tissue, deep adipose tissue, muscle, liver, or others.

occur exclusively in the liver, according to the following equation:

$$Deg.Flow\ PCB_{liver}\ \left(ng.d^{-1}\right) = A_{Liver} \times k_{met} \quad (3)$$

where A_{Liver} the amount of PCB in the *Liver* compartment (ng) and k_{met} is the first-order metabolism rate constant (d^{-1}).

2.1.3. Feed ingestion, lipid digestion, and growth physiology sub-models

Due to their lipophilic and apolar nature, PCBs preferentially accumulate into lipid-rich tissues. For modeling purposes, the BeefPOP model assumes that PCBs are almost exclusively distributed into body lipids. Their transport and distribution across the body compartments and fecal excretion are further assumed to be proportional to the flow and fate of lipids across body tissues and digestive contents all over the cow lifespan (MacLachlan, 2009). Accordingly, to simulate the PCB fluxes, mass exchanges, and concentrations within the ADME sub-model, it is essential to characterize the kinetics of total and lipid masses across all compartments. The lipid ingestion and digestion sub-model (represented in the green box in Fig. 1) describes the transfer of lipids from intake through the digestive tract, their apparent absorption into the organism, and the remaining fraction excreted in the feces, based on the INRA feeding system equations (INRA, 2018). The main parameters implemented in this sub-model are presented in Table 1, and the detailed equations are available in Supplementary Information S2.

Lipid ingestion originates from either solid feed or milk intake. For solid feed, lipid content is derived from the proportion of lipids (i.e.,

ether-extracted fat) in dry matter intake (DMI) using measured or estimated values (e.g., from INRA feed tables; INRA, 2018). The lipid content in milk is described by Martin and Sauvant's (2007) dynamic model, which detailed the physiology of the lactating cow modeled in Lerch et al. (2025). Lipids originating from solid feed flow from the *Feed* to the *Rumen* ($Q_{Feed\rightarrow Rumen}$) and further to the *Intestine* ($Q_{Rumen\rightarrow Intestine}$). For lipids originating from milk, an adjustment was made to reflect the esophageal groove reflex and represent the time of a suckling event (INRA, 2018), with a flow from *Milk* to the *Abomasum* and further the *Intestine* (see details in Supplementary Information S3). Once they enter the *Intestine*, the lipids are either absorbed ($Q_{Intestine\rightarrow absorbed}$) or excreted in feces ($Q_{Intestine\rightarrow Feces}$). The lipid quantity in the *Intestine* is dynamically computed by integrating lipid inflow from the *Rumen* and subtracting the absorbed and fecal excreted fractions.

The physiological sub-model representing the growth of beef cattle (in a blue box in Fig. 1) is based on the mechanistic model "MecSiC" initially developed by Hoch and Agabriel (2004a,b). The main parameters of the "MecSiC" model are presented in Table 1, and the corresponding equations are detailed in Supplementary Information S3. Briefly, the metabolizable energy (ME) from solid feed and milk intake is allocated to the syntheses of proteins and lipids in carcass and non-carcass compartments. The efficiency of these syntheses, as well as protein and lipid degradation, depends on the current carcass and non-carcass protein and lipid masses and is relative to the animal's developmental stage and category (i.e., body composition at maturity). Allometric equations are then used to convert the protein and lipid masses into carcass, empty body (EB), and full body weights.

To integrate the growth physiology sub-model into the BeefPOP model, additional allometric equations were established to estimate the total and lipid masses of body compartments represented in the ADME sub-model (i.e., *Blood*, *Liver*, *Muscles*, *Adipose tissues*, and *Others* compartments). These equations were developed from the INRA-Theix slaughterhouse database (https://doi.org/10.15454/1.5572318050509348E12; cited by Hoch and Agabriel, 2004a), which contains detailed anatomical and chemical composition data for 133 growing cattle (Supplementary Information S3, Table S3.2). Using these data, four allometric equations were applied to estimate tissue-specific total fresh and lipid masses based on simulated protein and lipid masses in carcass and non-carcass compartments. The relationships between carcass protein mass and muscle fresh mass, and between carcass and muscle lipid masses showed good agreement, with R^2 values of 0.99 and 0.88, respectively. Similarly, the relationship between EB lipid mass and adipose tissue fresh and lipid masses showed an R^2 of 0.99. Detailed equations and goodness-of-fit metrics are provided in Supplementary Information S3. Fixed proportions of EB water mass or EB weight were used to derive *Blood* and *Liver* masses, respectively.

2.1.4. Model implementation

The BeefPOP model was developed using the software Vensim® Professional version 9.3.2 (Ventana Systems, Inc.). The complete model file and code are available in an online data repository at https://doi.org/10.5281/zenodo.17600518. Numerical integration of the system of differential equations was performed using the fourth-order Runge-Kutta method, with a fixed time step of 1 min. Such temporal resolution reduced to 1 min was necessary to prevent numerical overflows during simulations, whereas only simulations at one day interval were extracted and interpreted.

2.2. Optimization and preliminary evaluation of the model's predictive capabilities for PCBs

2.2.1. Overview of the toxicokinetics in vivo experiment

The BeefPOP model was implemented for PCBs using data from the toxicokinetic experiment detailed by Driesen et al. (2022a,b). In brief, the study involved 12 gestating Simmental cows (6 primiparous and 6 multiparous) and their belonging calves from 109 ± 11.5 days before calving until 288 ± 4.5 days in milk. Three treatments were compared: a control treatment (CTL; $n = 4$ cows, 4 calves) fed a non-contaminated grass-silage diet; an exposed treatment (EXP; $n = 4$ cows, 4 calves) receiving grass silage mixed with PCB-contaminated soil; and a depurated treatment (DEC; $n = 4$ cows, 4 calves), which were switched to the CTL clean grass-silage diet, following exposure like EXP until 164 ± 4.4 days in milk. Calves were separated from their mothers within 10 hours of birth and received the milk of their corresponding dam, along with ad libitum water and uncontaminated hay, as well as concentrate from three months of age. Regarding calves' measurements and sampling, throughout the experiment, we monitored several metrics, especially BW, milk, and feed intake and composition, as well as fecal excretion. At 89 and 164 days of age, in vivo blood samples were obtained by venipuncture, and subcutaneous adipose tissue samples were obtained by biopsy of the tail head. At slaughter (288 days of age), we sampled postmortem blood at exsanguination, subcutaneous (tail head), intermuscular (at the 11th rib), and perirenal adipose tissues, the *rectus abdominis* and *longissimus thoracis* (9–11th ribs) muscles, and the liver. Data from two calves from the EXP treatment that died prematurely at 90 days of age were included in the model evaluation database only for muscle and liver, to provide an early-stage assessment of tissue PCB distribution, as no in vivo kinetic data were collected for these tissues. These 90-days calves' data were not used for model optimization. The analysis of dl-PCBs and ndl-PCBs was conducted at Empa (Dübendorf, Switzerland) in every sample (feed, milk, feces, blood, and tissues) by Q Exactive Orbitrap gas chromatography combined with high-resolution mass spectrometry, following the analytical method described by Driesen et al. (2022a). The dl-PCB TEQ concentrations were calculated based on toxicity-equivalent factors defined by the World Health Organization (WHO) in 2005 for each congener (Van den Berg et al., 2006). The dl-PCB WHO-TEQ sum is expressed in a mid-bound scenario, including value concentrations below the limit of detection (LOD) set to half the LOD.

2.2.2. Model simulation workflow for optimization and preliminary evaluation

Three sets of simulations, for every PCB congener ($n = 18$), were performed to represent the CTL, EXP and DEC treatments for calves. Simulations began at birth for EXP and CTL, and at 164 days of age for the DEC group and ended at 288 days of age (time of slaughter) for all. Data from the EXP group were allocated to the optimization of the model, while CTL and DEC groups were used for the preliminary evaluation of the model predictive capabilities. Observed solid feed and milk intake, nutrient composition and PCB concentrations, and initial estimated PCB body burdens (Driesen et al., 2022a,b) were used to configure the simulations for each treatment group. These inputs are detailed in Supplementary Tables S1 and S2 for solid feed, S3 and S4 for milk, and S5 for initial body burdens. At both optimization and evaluation steps, for model inputs, PCB concentrations below the LOD were substituted with half the LOD, to avoid excluding the congener entirely.

To match observed data from the toxicokinetic experiment, that serves for optimization and evaluation, the calf physiology (i.e., growth kinetic and body composition) was also defined based on the experimental records (Driesen et al., 2022a,b). The BW was implemented directly from measurements taken throughout the experiment. The EB weight and lipid mass records were measured postmortem following EB dissection, grinding and chemical analyses (Xavier et al., 2022) at 90 days of age ($n = 2$) and 288 days of age ($n = 10$). At birth, BW was assumed to equal EB weight, and EB lipid concentration was set at 4.5% (Robelin, 1986). Between these three time points (birth, 90 and 288 days of age), EB weight and lipid mass were interpolated linearly.

Regarding PCB absorption and fecal excretion, the initial PCB absorption rates (AR) simulated by the model were calculated for each congener as:

Table 2
Adjustment of the absorption rate (AR), decimal logarithm of the partition coefficient between octanol and water (log K_{ow}), adjustment of the coefficient of partition between blood and other tissues (*Corr* P_i), and metabolic first-order clearance rates in the liver (k_{met}) of non-dioxin-like polychlorinated biphenyl (ndl-PCB) and dioxin-like polychlorinated biphenyl (dl-PCB) congeners for the BeefPOP model simulations.

			Corr P_i[d] BeefPOP (unitless)				
PCB congener		AR correction factor (unitless)[a]	AT, Others[e]	Muscle[f]	Liver[g]	log K_{ow} (unitless)	k_{met} (d^{-1}) [i]
ndl-PCB							
	PCB 28	0.82	-[b]	2.53	4.30	5.6	4.5
	PCB 52	0.82	0.25	12.70	26.06	5.8	0.5
	PCB 101	0.78	0.15	6.77	15.57	6.3	0.5
	PCB 138	-[b]	-[b]	-[b]	7.76	6.7	0.1
	PCB 153	-[b]	-[b]	-[b]	4.18	6.8	0.0
	PCB 180	1.17	-[b]	-[b]	3.81	7.2	0.1
dl-PCB							
	PCB 77	-[b]	0.59	-[b]	2.98	6.4	9.4[j]
	PCB 81	-[c]	-[b]	2.10[h]	1.36[h]	6.4	6.2[j]
	PCB 105	-[b]	-[b]	1.83	3.72	6.6	0.1
	PCB 114	-[b]	-[b]	1.89	2.40	6.6	0.0
	PCB 118	-[b]	-[b]	-[b]	1.95	6.7	0.0
	PCB 123	-[b]	-[b]	1.44	2.55	6.7	0.9
	PCB 126	-[b]	-[b]	-[b]	3.71	7.0	0.1
	PCB 156	-[b]	-[b]	-[b]	-[b]	7.1	0.0
	PCB 157	-[b]	-[b]	-[b]	-[b]	7.1	0.0
	PCB 167	1.19	0.43	0.45	0.67	7.2	0.1
	PCB 169	1.25	-[b]	-[b]	-[b]	7.5	0.0[j]
	PCB 189	1.29	-[b]	-[b]	-[b]	7.6	0.0

Abbreviations: exposed treatment (EXP), adipose tissue (AT).
[a] The AR correction factors were only applied when simulating the case of the toxicokinetic experiment and were defined as the ratio between observed absorption rate (Driesen et al., 2022b) and initial model simulated absorption rate.
[b] No need for adjustment as the correction value was closed to 1.0 (between 0.9 and 1.1).
[c] The AR could not be determined as some values were below the limit of detection.
[d] The *Corr* P_i is defined as the ratio of lipid-normalized concentrations between *tissue i* and blood in calves from treatment EXP at 10 months of the experimental study (Driesen et al., 2022a; mean of $n = 3$) and is a multiplicative coefficient to be applied to the initial value of P_i defined by the ratio $Lipids_i$ *(% fresh mass)/* $Lipids_{blood}$ *(% fresh mass)*.
[e] Lipid-normalized concentration ratio between empty body and blood.
[f] Lipid-normalized concentration ratio between the mean of *longissimus thoracis* and *rectus abdominis* muscles and blood (unless stated with the [h] superscript).
[g] Lipid-normalized concentration ratio between liver and blood (unless stated with the [h] superscript).
[h] Blood concentration was lower than the limit of detection for the specific congener and empty body concentration was used instead as the *Corr* P_i denominator.
[i] Only the k_{met} was optimized for individual PCB congeners using the payoff function of Vensim®.
[j] Observed adipose tissue concentrations used for k_{met} optimization presented one or more values below the limit of detection and were converted to an estimated concentration defined at LOD/2 (mid-bound scenario). Values should be interpreted with caution.

$$Simulated\ absorption\ rate = \frac{PCB\ intake - PCB\ feces\ excreted}{PCB\ intake} \quad (4)$$

A correction factor was then determined as the ratio between the observed (Driesen et al., 2022b) and initially simulated AR and applied to the diet input to force the simulated PCB absorbed fraction to the experimental data (Table 2). Regarding PCB body distribution, the partitioning coefficients P_i were adjusted using experimental records from the EXP group at slaughter. To account for PCB tissue distribution that cannot be fully explained by the lipid-based model structure, a correction factor (*Corr* P_i, detailed in Table 2) was calculated for each tissue as the ratio of lipid-normalized PCB concentrations between tissue *i* and the *Blood* (or the EB if blood concentrations were below the LOD). This correction factor was then multiplied with the initial P_i (ratio of *tissue i* to blood lipid concentrations). Both AR and *Corr* P_i were not optimized parameters, but were considered fixed and identifiable from the experimental data. The K_{ow} values were obtained from the literature (Amutova et al., 2021). Finally, regarding PCB metabolism, the first-order metabolism rate constant (k_{met}) was the only parameter not identifiable from the experimental records, and was further optimized individually for the 6 ndl-PCBs and 12 dl-PCBs using the payoff function of Vensim® software. The model total *Adipose tissue* predictions, corresponding to the sum of *Perfused* and *Deep adipose tissue* compartments, were fitted to the average of observed subcutaneous, intermuscular, and perirenal adipose tissue concentrations at slaughter, or to subcutaneous adipose tissue when only in vivo samples were available, in calves from the EXP treatment (not including data from the two calves that died at 90 days old; Table 2). The optimized parameters were subsequently used in the final version of the model, which was then preliminarily evaluated by reproducing the CTL and DEC treatments. While the evaluation is not fully independent (i.e., data of the CTL and DEC calves were gathered from the same experiment as the EXP calves), individual physiological and intake data from these groups were not used in the calibration, providing a reliable preliminary assessment of model performances.

2.2.3. Quantitative assessment of the model's predictive capabilities

The predictive capabilities of the BeefPOP model were evaluated by comparing simulated and observed concentrations of PCBs in adipose tissues, muscles, and the liver of calves from the EXP group (used for model optimization) and from the DEC and CTL groups (used for model evaluation). In both cases, individual congeners were grouped into ndl- or dl-PCBs, and individual measurements below the limit of quantification were excluded for performance evaluation, as such values are considered less reliable. The evaluation of model adequacy focused on both accuracy, defined as the closeness of the model predictions to the observed values, and goodness of fit, which reflects the consistency of the model predictions. A comprehensive set of statistical indicators was used to assess model predictive capabilities (Tedeschi, 2006) using R software (version 4.3.2). Accuracy was assessed using mean bias (MB), defined as the average difference between predicted and observed values (Tedeschi, 2006), and mean absolute percentage error (MAPE), representing the average absolute deviation to observed means (Cheng et al., 2016). The accuracy of the model was considered satisfactory when the MB relative to the observed mean was equal to or below 25%,

and the MAPE was equal to or less than 50% (Li et al., 2018). The model's goodness of fit was quantified using the coefficient of determination (R^2) of the linear regression between predictions and observations, the root mean square error (RMSE), and the relative RMSE (RRMSE) (Tedeschi, 2006).

To further describe model performances, the RMSE was decomposed in error due to central tendency (ECT), which indicates bias, error due to regression (ER), reflecting the predictive consistency, and error due to disturbance (ED), capturing random variability (Tedeschi, 2006). A satisfactory model goodness of fit was defined by an R^2 equal to or higher than 0.75 (Li et al., 2018), an RMSE equal to or below the standard deviation of the observed mean, an RRMSE of 50% or less (Cheng et al., 2016), and an ED equal to or higher than 60%. Finally, both accuracy and goodness of fit were assessed by calculating the concordance correlation coefficient (CCC) and its decomposition into scale shift (ν), location shift (μ), and bias correction factor (C_b) (Tedeschi, 2006). Values were considered satisfactory when CCC and C_b were equal to or higher than 0.75.

2.3. Model simulation of diverse scenarios of beef production systems and PCB exposure

After optimization and evaluation of the 18 individual congeners of PCBs, the BeefPOP model was applied to prospective scenarios to explore PCB exposure and depuration toxicokinetics in growing and fattening beef cattle. Simulated scenarios accounted for differences in cattle category, growth rate, and sources of PCB contamination. Although the BeefPOP model may simulate PCB kinetics from birth to mature body weight, the prospective scenarios were initiated at 250 kg to illustrate the use of the model in specific cases representative of realistic beef fattening systems.

2.3.1. Scenarios of beef production systems

Two animal categories contrasted for maturity and body fatness were considered. Angus crossed Hereford steers represented very early-maturing cattle with high body fatness and high feed intake capacity, while Charolais bulls represented late-maturing cattle with a leaner body and moderate feed intake capacity. Model simulations of three different growth itineraries started at a BW of 250 kg and ended when animals reached a BW of 700 kg for a targeted hot carcass weight of around 400 kg. Their respective feed intake capacities were defined as allometric relationships based on BW, according to the equations from the INRA feeding system for each breed and rate of growth (INRA, 2018; Supplementary Table S6). The growth itineraries included a slow growth path (SG), a fast growth path (FG), and a compensatory growth path (CG), in which animals followed the SG diet until reaching a BW of 475 kg before switching to the FG finishing diet. To achieve such different growth rates, two diets reflecting common farming practices in beef meat production were defined. In the SG scenario and the initial part of the CG itinerary, cattle were fed a low-energy diet consisting of 70% poor-quality hay, 15% corn grain, and 1% sunflower meal, with an ME content of 9.0 MJ.kg^{-1} DM. In the FG scenario and finishing part of the CG itinerary, cattle were fed a high-energy diet composed of 60% corn silage, 23% corn gluten meal, 10% corn grain, and 7% soybean meal, with an ME content of 12.0 MJ.kg^{-1} DM (see Supplementary Table S6 for additional details).

2.3.2. Scenarios of PCB exposure routes

To simulate the realistic conditions of on-farm PCB exposure in beef cattle, three contamination scenarios were considered based on specific contamination sources and their respective congener profiles. In all cases, the diets' WHO-TEQ sum of dl-PCBs was set to the EU action level for feed of 0.40 ng TEQ.kg^{-1} DM (EU regulation No 277/2012). The ndl-PCB concentrations were estimated based on the relative proportions of ndl-PCBs to dl-PCBs for each exposure source. The first PCB exposure scenario (*Paint*) simulated a punctual source of exposure from ingested wall paint particles, representative of a real case of exposure to contaminated barn materials (Bogdal et al., 2017). This scenario applied the PCB congener pattern of contribution to the WHO-TEQ sum reported in the case of a suckler beef farm in Switzerland contaminated with PCB-containing wall paint (Bogdal et al., 2017). The diet level of exposure at 0.40 ng TEQ.kg^{-1} DM corresponds to a realistic paint intake of 3.8 mg.kg^{-1} total DM intake per day, based on the ratio between diet exposure level and wall paint concentration (Bogdal et al., 2017). The corresponding concentration for the sum of ndl-PCBs was of 104 μg.kg^{-1} DM.

The second scenario (*Feed*) represented a punctual source of exposure from industrial byproduct feedstuffs, specifically bread crumbs, using the PCB congener pattern reported by Heres et al. (2010). In this case, feed PCB contamination was linked to the use of PCB-contaminated burning oil for drying bakery waste in the Republic of Ireland. This feedstuff-based contamination corresponds to a bread crumb intake of 15 g.kg^{-1} total DM intake. The corresponding concentration for the sum of ndl-PCBs was 15.1 μg.kg^{-1} DM. The third scenario (*Soil*) described a diffusive source of exposure from soil ingestion using the PCB congener pattern reported by Fournier et al. (2013). In this case, a rural site near St Cyprien, France, was polluted by a fire on a PCB-contaminated site. This scenario would represent a soil ingestion of 9.5% of the total DM intake. The corresponding concentration for the sum of ndl-PCBs was of 1.03 μg.kg^{-1} DM.

Both the constant exposure scenario and an initial exposure followed by a depuration phase were simulated for each PCB exposure source. The depuration phase started after constant exposure until cattle reached 475 kg of BW, after which they were fed a clean diet with a background PCB level fixed at a WHO-TEQ sum of 0.04 ng TEQ.kg^{-1} DM for dl-PCBs and 0.23 μg.kg^{-1} DM for the sum of ndl-PCBs. The PCB level and congener pattern correspond to those commonly observed in forages, consistent with those observed in the CTL clean grass-silage diet described by Driesen et al. (2022a,b). Concentrations of dl-PCBs and ndl-PCBs in each contamination scenario and the depuration phase are detailed in Supplementary Table S7.

2.3.3. Quantification of PCB accumulation and depuration kinetics

To assess the accumulation rate of PCBs, bioconcentration factors (BCFs; Takaki et al., 2015) and assimilation efficiencies (AEs; Jondreville et al., 2017) were calculated separately for the sum of ndl-PCBs and the WHO-TEQ sum of dl-PCBs across all growth scenarios and contamination sources. The BCFs were determined for adipose tissues, muscles, and the liver using the following equation:

$$BCF\ (unitless) = \frac{[PCB]_{tissue_i}\ (ng.kg^{-1} lipids)}{[PCB]_{feed}\ (ng.kg^{-1} DM)} \quad (5)$$

with $[PCB]_{tissue\ i}$ the PCB concentration in the tissue at the end of the simulation (700 kg BW) for the constant exposure scenarios, and $[PCB]_{feed}$ the constant concentration in the total DM intake.

The AEs were calculated according to Equation (6):

$$AE\ (\%) = \frac{PCB\ body\ burden\ (ng)}{PCB\ total\ intake\ (ng)} \times 100 \quad (6)$$

where *PCB body burden* is the amount of PCB in the animal EB, and PCB total intake is the sum of PCB intake over the entire time span of the simulation.

During the depuration phase, the depuration half-lives ($t_{1/2}$) of PCB sums were determined in muscles and adipose tissues. The depuration decay of PCB concentration in muscles was modeled using a bi-exponential function to account for the two-phase depuration process, as follows:

$$C_t\ (ng.kg^{-1}\ lipids) = a \times e^{-\alpha t} + b \times e^{-\beta t} \quad (7)$$

where C_t is the PCB concentration at time t, a and b are the initial concentrations for the fast and slow depuration compartments, respectively,

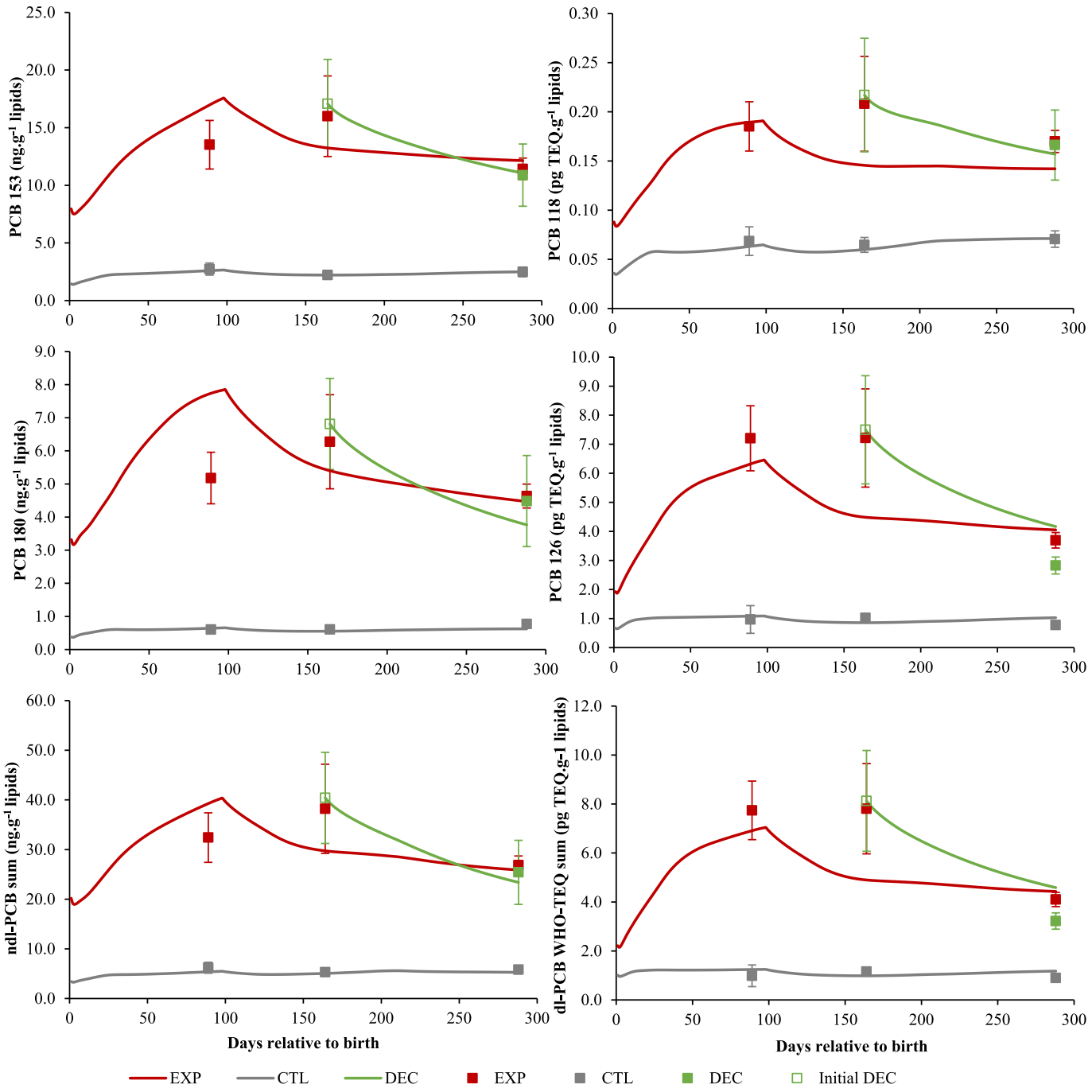

Fig. 2. Concentrations of non-dioxin-like polychlorinated biphenyl (ndl-PCB) and dioxin-like polychlorinated biphenyl (dl-PCB) kinetics in adipose tissues of calves from biological observations compared to simulations by BeefPOP, the physiologically based toxicokinetic model. The adipose tissue concentrations of PCB 153, PCB 180, ndl-PCB sum, PCB 118, PCB 126, and dl-PCB sum in toxic-equivalent according to the World Health Organization in 2005 (WHO-TEQ sum) of the BeefPOP model simulations in comparison to the biological observations previously published (Driesen et al., 2022a) are displayed for exposed (EXP), control (CTL), and depurated (DEC) calves.

and α and β are the short and long phase decay constants (d^{-1}), respectively.

For the adipose tissues, a mono-exponential decay model was used, corresponding to the long (β) phase only. For each PCB congener, the onset of the mono-exponential depuration in adipose tissues was set at five time the α half-life previously determined in muscles. The half-life ($t_{1/2}$) was further defined as follows:

$$t_{1/2_{\alpha \text{ or } \beta}}(d) = \frac{\ln(2)}{\alpha \text{ or } \beta} \quad (8)$$

3. Results

3.1. Optimization and preliminary evaluation of the model's predictive capabilities for PCBs against observations from an in vivo toxicokinetic experiment

3.1.1. Qualitative assessment of the model's fit

Fig. 2 shows a comparison of previously published biological observations (Driesen et al., 2022a) and the model's simulations of PCB concentrations in adipose tissues for the three experimental treatments.

Table 3
Summary of statistical indicators of the adequacy (accuracy and goodness-of-fit) of the BeefPOP model for the predictions of adipose tissue, muscle, and liver concentrations in non-dioxin-like polychlorinated biphenyls (ndl-PCBs) and dioxin-like polychlorinated biphenyls (dl-PCBs) during the toxicokinetic experiment.

Tissue	Congener	Treatment	n	Mean ± standard deviation (pg g^{-1} lipids)		MB	R^2	Model efficiency	MAPE (%)	RMSE	RRMSE (%)	ECT (%)	ER (%)	ED (%)	CCC	v	μ	C_b
				Observed	Predicted													
Adipose tissue																		
	ndl-PCB[a]																	
		EXP	10	9.69 ± 5.36	9.42 ± 5.12	-0.27	0.79	0.78	19.19	2.37	24.46	1.32	0.89	97.79	0.89	0.96	-0.06	1.00
		DEC, CTL	16	2.64 ± 3.26	2.41 ± 3.09	-0.23	0.99	0.98	18.17	0.45	17.24	25.09	13.52	61.39	0.99	0.95	-0.07	1.00
	dl-PCB[b]																	
		EXP	30	0.65 ± 1.90	0.54 ± 1.53	-0.11	0.95	0.92	17.55	0.53	80.65	4.63	48.08	47.29	0.95	0.80	-0.07	0.98
		DEC, CTL	39	0.16 ± 0.50	0.20 ± 0.70	0.04	0.98	0.80	12.42	0.22	137.25	3.22	80.47	16.31	0.93	1.40	0.07	0.94
Muscle																		
	ndl-PCB[a]																	
		EXP	12	10.92 ± 7.05	6.71 ± 6.34	-4.21	0.24	-0.31	43.13	7.73	70.77	29.63	0.78	69.59	0.40	0.90	-0.66	0.82
		DEC, CTL	12	3.77 ± 3.44	3.52 ± 3.41	-0.25	0.89	0.88	40.77	1.13	29.87	4.99	0.06	94.95	0.94	0.99	-0.08	1.00
	dl-PCB[b]																	
		EXP	24	0.48 ± 1.46	0.53 ± 1.65	0.05	0.99	0.98	49.67	0.20	42.53	7.26	87.37	5.38	0.99	1.13	0.04	0.99
		DEC, CTL	23	0.16 ± 0.51	0.27 ± 0.94	0.11	0.99	0.20	56.72	0.45	278.59	6.58	91.06	2.36	0.82	1.86	0.17	0.83
Liver																		
	ndl-PCB[a]																	
		EXP	12	25.12 ± 29.13	33.42 ± 39.73	8.30	0.46	-0.09	77.09	29.18	116.15	8.09	12.10	79.82	0.63	1.36	0.26	0.93
		DEC, CTL	12	16.65 ± 16.80	15.46 ± 20.67	-1.19	0.98	0.92	35.71	4.59	27.56	6.76	65.21	28.03	0.97	1.23	-0.07	0.98
	dl-PCB[b]																	
		EXP	24	0.93 ± 3.00	1.86 ± 6.15	0.92	0.91	-0.40	65.17	3.47	372.10	7.10	79.36	13.55	0.74	2.05	0.22	0.77
		DEC, CTL	24	0.47 ± 1.68	0.92 ± 3.43	0.45	0.99	-0.17	57.12	1.78	376.74	6.37	93.48	0.14	0.78	2.04	0.19	0.78

Abbreviations: toxic equivalent (TEQ), exposed treatment (EXP), depurated treatment (DEC), control treatment (CTL), number of observations (n), mean bias (MB), coefficient of determination (R^2), mean absolute percentage error (MAPE), root mean square error (RMSE), relative root mean square error to the observed mean (RRMSE), proportion of error due to central tendency (ECT), proportion of error due to regression (ER), proportion of error due to disturbance (ED), concordance correlation coefficient (CCC), decomposed CCC to estimate the scale shift (v), decomposed CCC to estimate a location bias relative to the scale shift (μ), decomposed CCC to estimate a bias correction factor (C_b).
Cells highlighted in green are indicative of satisfactory model goodness of fit, with absolute MB relative to the observed mean $\leq$ 25%, MAPE $\leq$ 50%, R^2 and model efficiency $\geq$ 0.70, RMSE $\leq$ standard deviation of the observed mean, RRMSE $\leq$ 50%, ED $\geq$ 60%, CCC and $C_b \geq$ 0.75.
[a] 6 ndl-PCB congener concentrations in ng.g^{-1} lipids.
[b] 12 dl-PCB congener concentrations in pg TEQ.g^{-1} lipids.

For illustration purposes, PCB 153 and 180 were selected for their high contribution to the ndl-PCB sum and their distinct physicochemical properties (i.e., K_{ow} and k_{met}), while PCB 118 and 126 were chosen for their major contributions to the raw sum and WHO-TEQ sum of dl-PCB, respectively.

In both the optimization (EXP treatment) and preliminary evaluation (DEC and CTL treatments) steps, the model successfully reproduced the accumulation and depuration kinetics in adipose tissues, as the predictions aligned well with the observed concentrations at different time points (89, 164, and 288 days of age). At 164 days of age, the model tended to slightly underestimate concentrations in adipose tissues ndl-PCB and dl-PCB WHO-TEQ sums, but overall deviations between the predicted and observed values remained below 1.4-fold. The model's predictions of the ndl-PCB and dl-PCB WHO-TEQ sums showed satisfactory results, particularly at the end of the simulation (288 days of age). The maximum deviation at 288 days of age was observed in the dl-PCB prediction for the DEC treatment, with the model-predicted concentrations 1.4-fold higher than the observations. However, for the EXP and CTL treatments at this time point, the model predictions were generally within 1.1-fold of the observed values. Additional results for muscle and liver PCB concentrations are provided in Supplementary Figs. S1 and S2, similarly showing satisfactory agreement between model predictions and biological observations. Furthermore, the model's ability to fairly reproduce the congener-specific contributions to the total PCB sums in adipose tissues is illustrated in Supplementary Fig. S3.

3.1.2. Quantitative assessment of the model's predictive capabilities

The statistical indicators of BeefPOP model adequacy are presented in Table 3. Fig. 3 also shows linear regressions between the observed and predicted concentrations for individual ndl-PCB and dl-PCB congeners in adipose tissues. Linear regressions for muscles and the liver are detailed in Supplementary Figs. S4 and S5, respectively. Supplementary Fig. S6 summarizes the regression outcomes for the sums of ndl-PCBs and dl-PCBs across all tissues. In addition, Supplementary Fig. S7 presents the $\log_{10}$-scale residual plot of BeefPOP model predictions of ndl- and dl-PCB predictions in adipose tissue, muscle and liver. For both the optimization (EXP treatment) and the preliminary evaluation (DEC and CTL treatments) steps, the model demonstrated satisfactory goodness of fit. In adipose tissues, R^2 exceeded 0.79 for both ndl-PCBs and dl-PCBs for all treatments. The RMSE was consistently below the standard deviation of the observed mean. The ndl-PCB predictions showed satisfactory RRMSE of 25% and 17% for the EXP and DEC/CTL treatments, respectively, with the ED accounting for over 60% of the RMSE. By contrast, predictions of dl-PCBs had higher RRMSE values (81% and 137% for EXP, and DEC/CTL, respectively), with a lower contribution of ED to the RMSE. In terms of accuracy, all treatments (EXP and DEC/CTL) indicated minimal deviations between the predicted and observed values, with an absolute MB lower than 25% of the observed mean. For both ndl-PCBs and dl-PCBs, the BeefPOP model presented MAPEs below 20%. Additionally, the CCC was satisfactory, with values close to 1 in all cases. Its decomposition further showed a C_b ranging from 0.94 to 1.00, indicating minimal bias.

For muscles and the liver, which were not directly included in the optimization phase, the model showed variable performances. Adequacy was satisfactory overall, with R^2 exceeding 0.89 for most predictions of PCBs in the DEC/CTL treatments. However, a lower R^2 was observed for ndl-PCBs in the EXP treatment, with values of 0.24 in the muscles and 0.46 in the liver, and the values of RMSE and RRMSE were higher. In particular, liver RRMSE for dl-PCBs exceeded 370% for both

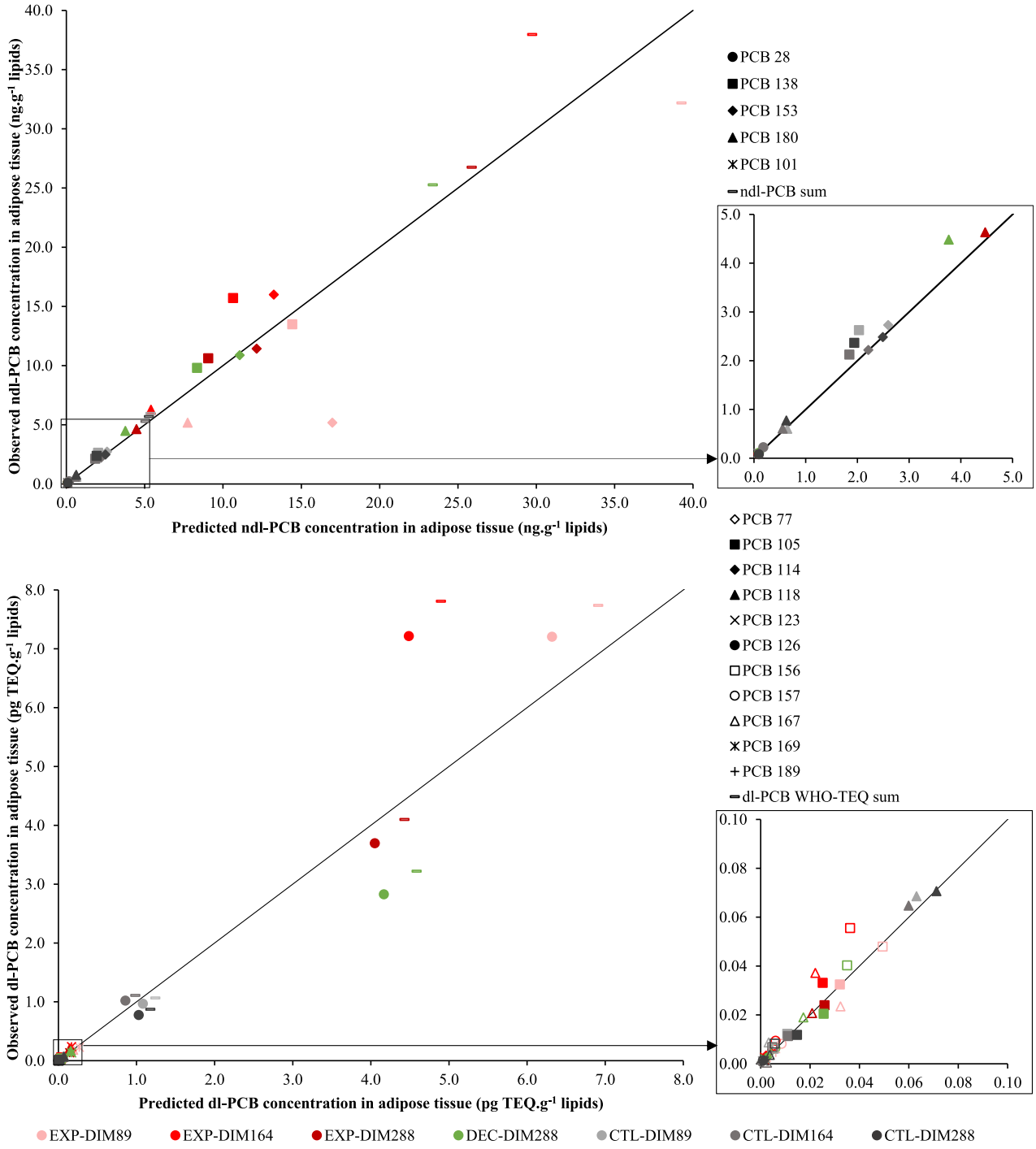

Fig. 3. Linear regression of non-dioxin-like polychlorinated biphenyl (ndl-PCB) and dioxin-like polychlorinated biphenyl (dl-PCB) congener concentrations in adipose tissues based on biological observations compared to simulations by BeefPOP, the physiologically based toxicokinetic model. The adipose tissue PCB congener concentrations simulated by the BeefPOP model compared to biological observations previously published (Driesen et al., 2022a) are displayed for exposed (EXP), control (CTL), and depurated (DEC) calves on different days relative to calving (DIM). For congeners PCB 52 and PCB 81, all biological measurements were below the limit of quantification and were therefore excluded.

the EXP and DEC/CTL treatments. Accuracy was generally acceptable in muscles, and was more variable in the liver. The MAPE values ranged from 41% (ndl-PCBs – DEC/CTL treatments) to 57% (dl-PCBs – DEC/CTL treatments) in the muscles and from 36% (ndl-PCB – EXP treatment) to 77% (ndl-PCBs – DEC/CTL treatments) in the liver. Despite this, the CCC ranged from 0.74 to 0.99 across all tissues and PCB congeners, with C_b values consistently close to 1, indicating limited systematic bias.

3.2. Model simulation of PCB contamination in diverse beef production systems and exposure scenarios

3.2.1. Effect of cattle category on physiological traits

Model simulations of the main physiological traits influencing the ADME of PCBs are presented in Supplementary Fig. S8 (DMI, BW, and hot carcass mass) and Supplementary Fig. S9 (lipid and protein masses

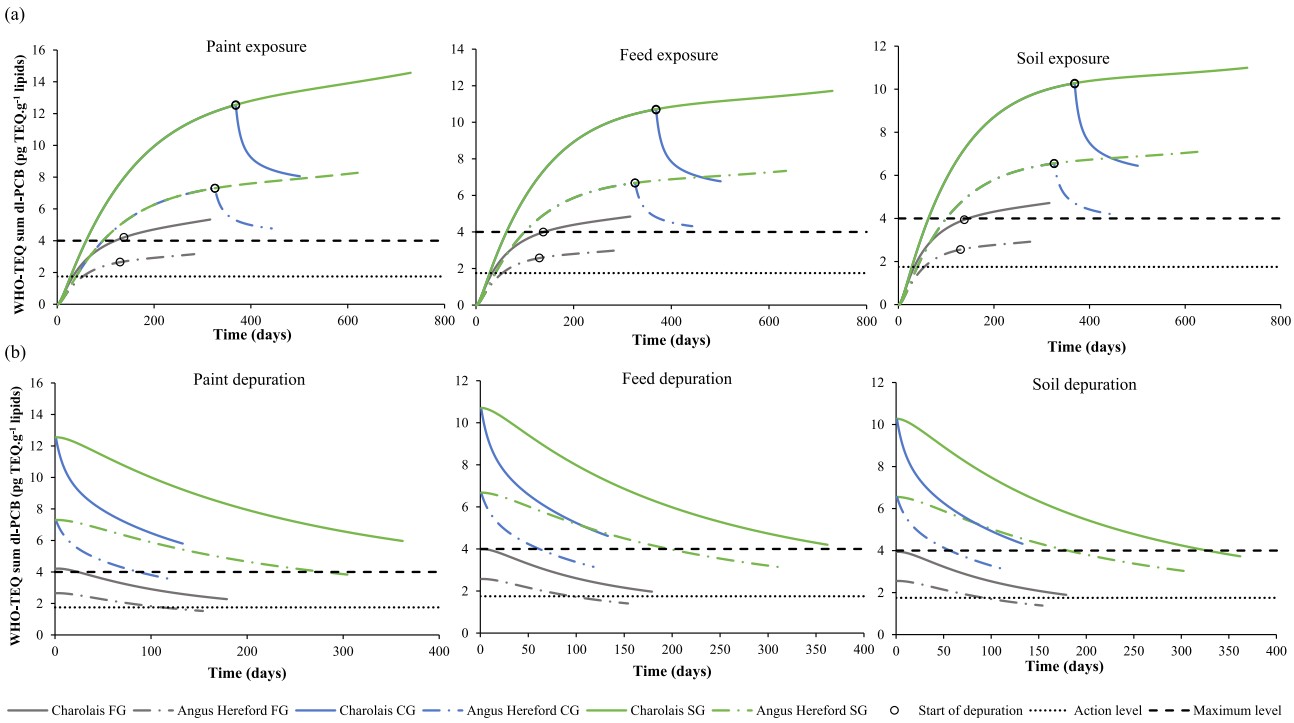

Fig. 4. Model simulations of dioxin-like polychlorinated biphenyl (dl-PCB) concentrations in the adipose tissue of growing cattle under different growth itineraries and PCB contamination sources. Model simulations are displayed for Charolais bulls and Angus × Hereford steers along slow growth (SG), fast growth (FG), and compensatory growth (CG) itineraries from 250 to 700 kg body weight. The upper panel displays constant exposure to PCB sources, presenting a congener profile from either wall paint (Paint, Bogdal et al., 2017), contaminated feed with Arochlors (Feed, Heres et al., 2010), or soil from a PCB-contaminated area (Soil, Fournier et al., 2013), with a total diet concentration of dl-PCB set at 0.40 ng TEQ.kg^{-1} dry matter. The ndl-PCB sum in the total diet was 104, 15.5, and 1.03 μg.kg^{-1} dry matter for the Paint, Feed and Soil sources of exposure, respectively. The depuration phase (lower panel) was initiated at 475 kg body weight (i.e., from time point illustrated by ○ symbols on the exposure upper panel), with a diet at a PCB concentration and congener profile corresponding to background level: dl-PCB concentration of 0.04 ng TEQ.kg^{-1} dry matter and ndl-PCB concentration of 0.23 μg.kg^{-1} dry matter.

in the carcass). Simulations were performed for two categories of cattle, Charolais bulls and Angus × Hereford steers, under three growth itineraries: slow, fast, and compensatory growth. Across all scenarios, Charolais bulls took approximately 1.1 times longer to reach the target BW of 700 kg compared to the Angus × Hereford steers. The average daily gains of the Charolais bulls were 0.62, 1.42, 0.61, and 1.66 kg.d^{-1} under the SG, FG, CG before refeeding (before 475 kg BW), and CG after refeeding scenarios, respectively. For the Angus × Hereford steers, the corresponding average daily gains were 0.71, 1.60, 0.69, and 1.88 kg.d^{-1}, respectively, under these scenarios. The DMI was consistently higher in the Angus × Hereford steers (1.1-fold higher in SG and CG before refeeding, and 1.2-fold higher in FG and CG after refeeding scenarios), while the EB weight did not present relevant differences between animals. Regarding carcass composition, the Charolais bulls had a protein mass 1.3-fold higher and lipid mass 1.9-fold lower than those of the Angus × Hereford steers. Charolais carcasses also contained nearly equal amounts of proteins and lipids, while Angus × Hereford carcasses had approximately 2.5 times more lipids than proteins.

3.2.2. *Effect of cattle category, growth rate, and source of exposure on PCB accumulation kinetics*

Fig. 4a illustrates BeefPOP model simulations of dl-PCB WHO-TEQ sum accumulation after constant exposure in adipose tissues of the Charolais bulls and Angus × Hereford steers under three growth itineraries (SG, FG, and CG) and according to three exposure sources (*Paint*, *Feed* and *Soil*; $n = 18$ scenarios). Each constant exposure scenario used a diet concentration of dl-PCB sum set at 0.40 ng TEQ·kg^{-1} DM (action level of dl-PCBs in feed; EU regulation No 277/2012). During the exposure phase, dl-PCB concentrations in adipose tissues starting at 0 pg.g^{-1} lipids, increased steadily over time for every scenario. Across all scenarios, the final concentration of dl-PCBs in adipose tissues exceeded the ML of 4.0 pg TEQ.g^{-1} lipids for the sum of PCDD/Fs and dl-PCBs in ruminant meat (EU regulation No 1259/2011), except for the Angus × Hereford steers under the FG scenario. Considering the same exposure source, SG resulted in higher adipose tissue dl-PCB concentrations compared to the FG and CG scenarios. The Charolais bulls also showed higher dl-PCB concentrations than Angus × Hereford steers, with dl-PCB WHO-TEQ sum being, on average, 1.2-, 1.3-, and 1.4-fold higher in adipose tissues of Charolais for FG, CG, and SG scenarios, respectively. The ndl-PCB sums in adipose tissues showed similar accumulation patterns within each exposure source (detailed in Supplementary Fig. S10). Supplementary Figs. S11 and S12 display the kinetics of ndl-PCBs and dl-PCBs in the muscles and liver, respectively. Muscle and liver PCB patterns of accumulation kinetics were similar to those observed in adipose tissues. On average, PCB concentrations in muscle lipids were 1.4-fold and 1.2-fold higher than in adipose tissue for ndl-PCBs and dl-PCBs, respectively. In the liver, across all exposure scenarios, PCB concentrations exceeded the ML of 0.5 pg TEQ.g^{-1} wet weight for the sum of PCDD/Fs and dl-PCBs, and 3.0 ng.g^{-1} wet weight for ndl-PCBs (EU regulation No 1067/2013).

The BCFs and AEs of the ndl-PCBs and dl-PCBs across all scenarios ($n = 18$) are summarized in Table 4. The BCFs were consistently higher in the liver than in the muscles and adipose tissues. For ndl-PCBs, liver BCFs ranged from 59 to 155, and for dl-PCBs, the values ranged from 30 to 111. The Angus × Hereford steers generally showed lower BCFs compared to the Charolais bulls across all tissues and exposure sources. The BCFs were also lower in the FG scenarios than in the SG and CG scenarios. Overall, for ndl-PCBs, higher BCFs were observed under *Soil* exposure, while for dl-PCBs, *Paint* exposure resulted in the highest BCFs. The AEs ranged from 45% to 78%, with the highest value observed in the Angus × Hereford steers for dl-PCBs under the SG and *Paint* exposure scenario. The Angus × Hereford steers consistently showed higher AEs

Table 4
Non-dioxin-like polychlorinated biphenyls (ndl-PCBs) and dioxin-like polychlorinated biphenyls (dl-PCBs) bioconcentration factors in muscle, adipose tissue, and liver, assimilation efficiency in the total empty body, bi-exponential short (α) and long (β) half-lives in muscle, and mono-exponential depuration half-life in adipose tissue of growing Charolais bulls or Angus × Hereford steers under different growth itineraries[a] and PCB contamination sources[b].

	Charolais bulls									Angus × Hereford steers								
Growth itinerary	Slow growth			Fast growth			Compensatory growth			Slow growth			Fast growth			Compensatory growth		
PCB source	*Paint*	*Feed*	*Soil*	*Paint*	*Feed*	*Soil*	*Paint*	*Feed*	*Soil*	*Paint*	*Feed*	*Soil*	*Paint*	*Feed*	*Soil*	*Paint*	*Feed*	*Soil*
Bioconcentration factor[c] muscle																		
ndl-PCB	32	30	34	16	15	16	20	18	20	24	23	25	13	13	13	16	16	16
dl-PCB	43	34	31	18	16	15	25	20	19	29	25	24	14	13	12	18	16	16
Bioconcentration factor[c] adipose tissue																		
ndl-PCB	26	23	29	11	10	12	15	13	16	16	15	17	7	6	7	9	10	10
dl-PCB	36	29	27	13	12	12	20	17	16	21	18	18	8	7	7	12	11	11
Bioconcentration factor[c] liver																		
ndl-PCB	147	137	155	72	70	74	90	85	94	110	106	114	60	59	60	71	74	72
dl-PCB	86	105	111	38	50	54	51	64	68	61	80	85	30	41	44	52	55	53
Assimilation efficiency[d] (%)																		
ndl-PCB	52	46	58	48	45	47	50	45	54	60	56	65	52	49	55	57	53	61
dl-PCB	72	58	55	59	54	47	66	55	53	78	69	66	60	56	55	70	63	62
α half-life muscle[e]																		
ndl-PCB	30	29	50	17	17	21	13	13	13	30	30	38	13	13	13	15	14	15
dl-PCB	61	58	56	23	22	22	13	13	13	38	36	35	10	10	10	15	15	15
β half-life muscle[e]																		
ndl-PCB	260	25	614	142	142	336	140	133	202	244	343	380	119	117	253	119	115	193
dl-PCB	438	358	327	233	205	197	181	159	152	370	320	304	201	193	191	167	154	150
Half-life adipose tissue[f]																		
ndl-PCB	261	248	561	148	147	293	156	150	203	252	249	464	131	227	152	141	150	197
dl-PCB	443	354	322	231	200	191	194	169	161	371	320	304	180	180	181	185	171	167

[a] The growth rate was either continuously slow with low-energy diet and an average daily body weight gain of 0.70 kg, continuously fast with high-energy diet and an average daily body weight gain of 1.5 kg, or discontinuously slow and further fast with compensatory growth and average daily body weight gains of 0.65 kg during the slow growth and 1.8 kg during the fast growth. For every cattle category and growth itinerary, initial and final slaughter body weights were 250 and 700 kg, respectively.

[b] The source of oral exposure to PCBs shows a congener profile from either wall paint (*Paint*, Bogdal et al., 2017), contaminated feed with PCB transformer oil (*Feed*, Heres et al., 2010), or soil from a PCB-contaminated area (*Soil*, Fournier et al., 2013), with a total diet concentration for the sum dl-PCB sets at 0.40 ng TEQ·kg^{-1} DM (action level in feed, EU regulation No 277/2012). The respective ndl-PCB sum in the diet were 104, 15.5, and 1.03 μg.kg^{-1} dry matter in the total diet for the *Paint*, *Feed*, and *Soil* sources of exposure, respectively.

[c] Bioconcentration factor is defined for the constant exposure scenarios as the ratio of PCB concentration in tissue *i* at slaughter (pg.g^{-1} lipids) to the one in the diet (ng.kg^{-1} dry matter).

[d] Assimilation efficiency is defined for the constant exposure scenarios as follows: Assimilation efficiency (%) = body burden at the time of slaughter (ng) / total oral intake along the whole exposure phase (ng) × 100.

[e] A bi-exponential decay model [$C_t = a \times \exp(-\alpha \times t) + b \times \exp(-\beta \times t)$] was fitted to the muscle PCB concentration during the depuration phase, initiated at 475 kg body weight, with a diet showing PCB concentration and congener profile corresponding to background levels: dl-PCB concentration of 0.04 ng TEQ.kg^{-1}dry matter and ndl-PCB concentration of 0.23 μg.kg^{-1} dry matter. The α and β half-lives represent the short and long exponential compartments, and are calculated as ln(2)/α and ln(2)/β, respectively.

[f] A mono-exponential decay model [$C_t = b \times \exp(-\beta \times t)$] was fitted to the adipose tissue PCB concentration during the depuration phase, with data kinetic starting at 5 times the α half-life of the muscle. The half-life is calculated as ln(2)/β.

compared to the Charolais bulls (on average, 1.3-fold higher), and the SG itinerary was associated with higher AEs. Regarding the source of exposure, *Soil* exposure led to the highest AEs for ndl-PCBs, while *Paint* exposure resulted in higher AEs for dl-PCBs.

Finally, Supplementary Fig. S13 illustrates the profile of PCB congeners in the diet and adipose tissues of the Charolais bulls and Angus × Hereford steers under all exposure scenarios. For dl-PCBs expressed in raw concentrations, PCB 118 was the most abundant congener in *Paint*, *Feed* and *Soil* (39, 48, and 38%, respectively), followed by PCB 156 (33, 24, and 17%, respectively). When expressed in WHO-TEQ, *Paint* exposure showed high contributions from PCB 118 (24%), PCB 126 (35%), and PCB 156 (20%), while *Feed* and *Soil* exposures were dominated by PCB 126 (81% and 96%, respectively). The congener pattern observed in the adipose tissues was in close agreement with that of the diet. Regarding ndl-PCB, all sources of exposure presented similar patterns, with high contributions of PCB 138, PCB 153, and PCB 180 and, to a lesser extent, PCB 101, while the respective contribution of PCB 153 increased and that of PCB 101 decreased in adipose tissues.

3.2.3. *Effect of cattle category, growth rate, and source of exposure on PCB depuration kinetics*

A depuration phase was initiated at 475 kg BW using a diet with a dl-PCB concentration of 0.04 ng TEQ·kg^{-1} DM that led to a decrease in dl-PCB concentrations in adipose tissues (Fig. 4b). The rate of depuration varied according to the growth rate and previous source of exposure. Regarding the growth rate, the SG scenario showed a slower decline dl-PCB concentrations in adipose tissue compared to the CG and FG scenarios. Although both the SG and CG scenarios showed similar final dl-PCB concentrations in adipose tissue, the CG depuration phase was 2.7-fold shorter than SG for both the Charolais bulls and Angus × Hereford steers. After depuration, dl-PCB adipose tissue concentrations decreased below the ML for the Angus × Hereford steers in all growth scenarios and sources of exposure. For Charolais bulls, however, only the FG itinerary exposed to any sources, as well as the SG itinerary previously exposed through *Soil*, led to dl-PCB concentrations in adipose tissue below the ML. For ndl-PCBs, the depuration phase led to a slight decrease, but concentrations remained above the ML for *Paint* and *Feed* exposures, regardless of cattle category and growth itinerary (Supplementary Fig. S10). The liver and muscles showed rates of depuration comparable to those of adipose tissues (Supplementary Figs. S11 and S12, respectively).

The depuration kinetics demonstrated mono-exponential half-lives in adipose tissue ranging from 131 to 560 days for ndl-PCB, and from 161 to 442 days for dl-PCB, close to those for the long-term β half-lives

observed in muscles (Table 4). Muscles short-term α half-lives were shorter, ranging from 10 to 61 days, whereas long-term β half-lives varied from 115 to 614 days. Overall, the SG itinerary presented longer dl- and ndl-PCB half-lives compared to the FG and CG scenarios. The half-lives of the dl-PCBs were longer following *Paint* exposure, whereas those the ndl-PCBs were highest after *Soil* exposure.

4. Discussion

The use of PBTK models has emerged as a promising approach for estimating the transfer and accumulation of POPs such as PCBs in livestock (Moenning et al., 2023b; Mi and Lin, 2025). These models offer insights into the kinetics of contaminants, making them valuable tools for risk assessment and management (EFSA, 2014). As part of the new approach methodologies (Sewell et al., 2024), PBTK models contribute to more efficient resource use while reducing the reliance on in vivo testing, supporting the principles of replacement and reduction in animal experimentation (3Rs, Klevenhusen et al., 2021). Most preexisting PBTK models have been developed for specific contaminants and experimental contexts, limiting their applicability to broader scenarios (Lautz et al., 2019). For extensive use and accurate risk assessment, models should be physiologically relevant and adaptable to specific animal, herd characteristics, and feeding systems, including parameters such as DMI, BW, or body lipid mass, as highlighted by Moenning et al. (2023a) and Mi and Lin (2025). The value of a detailed and flexible description of the physiology to simulate various scenarios has been demonstrated for lipophilic contaminants, notably in dairy cows (Lerch et al., 2025), and growing broiler chickens (Méda et al., 2020). However, no such application currently exists for growing beef cattle, despite the importance of this production system, given the significant contribution of beef meat to human exposure to PCBs (EFSA, 2018). Moreover, PBTK models should provide congener-specific rather than sum predictions, and they should be evaluated for predictive capabilities to reliably estimate the transfer of the full spectrum of lipophilic contaminants.

In this context, the BeefPOP model introduced in the present study represents a major step forward. Developed for growing and fattening beef cattle, BeefPOP integrates fugacity and PBTK concepts with a fine description of physiological traits to reflect the biological processes driving the ADME of lipophilic contaminants in a generic and mechanistic approach. In this study, the model was optimized and evaluated for the 18 PCB congeners regulated in feed (EU regulation No 277/2012) and food (EU regulation No 1259/2011), including 6 ndl-PCBs and 12 dl-PCBs. At optimization and evaluation steps, AR and tissue partition were corrected using observed data from calves of the toxicokinetic experiment (fecal mass balance for AR, lipid-normalized tissue-to-blood ratios for *Corr* P_i; Driesen et al., 2022a,b). By fixing these identifiable parameters to the experimental records, only the k_{met} parameter was optimized to reproduce adipose tissue kinetics. While a full structural identifiability could not be formally demonstrated with the available dataset, this approach strengthens the identifiability of the k_{met} parameter and limit the risk of parameters compensation. Model performances were assessed using both non-steady-state and nearly steady-state experimental data, along the constant exposure or depuration phase, combining qualitative and quantitative evaluation methods. Furthermore, the model's ability to reproduce specific and realistic exposure cases was demonstrated, improving researchers' mechanistic understanding of ADME and physiological drivers. Our BeefPOP simulations also provide risk assessors and managers with a tool for the realistic estimation of contaminants levels on a case-by-case basis.

Some limitations of the model remain, and its parameters would require further development, particularly regarding the understanding of tissue transfer dynamics, especially in the liver. The current model assumes static partitioning, which may not fully capture physiological changes related to growth and maturity. A better understanding of dynamic partitioning processes and contaminant kinetics within adipose tissues is also needed to improve model adequacy and genericity. Moreover, integrating new approach methodologies (e.g., in vitro data) would enable refinement, for example, of the model parameters of metabolic and distribution processes. Finally, model predictions are deterministic and do not incorporate variability nor uncertainty on parameter estimates. Integrating uncertainty could be considered in future developments (e.g., using Monte Carlo simulations; Li et al., 2018). These advancements would establish BeefPOP as a flexible and robust tool for integrating new knowledge and covering an increasing range of contaminants, including emerging or remerging ones for which the availability of in vivo toxicokinetic data in beef cattle are scarce or non-existing (e.g., polychlorinated alkanes or naphthalenes).

4.1. Optimization and preliminary evaluation of the model's predictive capabilities for PCBs

Among the BeefPOP model parameters, only the first-order metabolism rate constant (k_{met}) was optimized using the in vivo data of the EXP treatment provided by Driesen et al. (2022a). Optimized k_{met} values were the highest for the low-chlorinated PCB 28, 77, and 81 (4.5, 9.4, and 6.2 d^{-1}, respectively), while most of the other congeners presented low to null k_{met} values (0 to 0.1 d^{-1}). A clear decreasing trend in k_{met} was observed when the degree of chlorination and lipophilicity (K_{ow}) of the PCB increased, in accordance with residual metabolic fractions estimated from the mass balance reported in calves by Driesen et al. (2022b). Overall, the k_{met} optimization aligns well with the metabolic susceptibility of PCBs, which depends on their chemical structure, especially their degree of chlorination (McLachlan, 1993; Thomas et al., 1999). In addition, the pattern of k_{met} values in the BeefPOP model was comparable to that of lactating cows in Lerch et al.'s (2025) RuMoPOP model and Bogdal et al.'s (2017) model, where lower chlorinated congeners also showed a high metabolism rate constant. An exception was observed for PCB 52 and PCB 101, both presenting high k_{met} in cows (394 and 324 d^{-1}, respectively, Lerch et al., 2025), but metabolized slowly in the BeefPOP model optimized with calf data (0.5 d^{-1}). Parallel optimization of the BeefPOP model without adjusting tissue partition coefficients (i.e., *Corr* $P_i = 1$; data not shown) was performed to allow a direct comparison of k_{met} absolute values with those of lactating cows in the RuMoPOP model (Lerch et al., 2025). The corresponding k_{met} values were still systematically lower in calves, which is in agreement with the reduced metabolization in young calf, especially under the age of 3 months, when compared to adult cows, as highlighted by Driesen et al. (2022b). The decrease of k_{met} values in calves with increasing PCB chlorination degree was also consistent with the in vivo records of higher biotransfer factors reported for higher chlorinated PCBs in adipose tissues of growing beef cattle (Driesen et al., 2021) and milk of dairy cows (reviewed by Amutova et al., 2021), suggesting lower metabolization. In accordance, PCBs with higher k_{met} values (e.g., PCB 28 and 77) also presented lower transfer factors in vivo (Driesen et al., 2021; Amutova et al., 2021).

The model's predictive capabilities were further evaluated against the optimization and additional evaluation datasets from the toxicokinetic experiment (Driesen et al., 2022a), using both visual appreciation and quantitative statistical indicators. Overall, the model demonstrated satisfactory performance in predicting adipose tissue PCB accumulation and depuration kinetics. Compared to Bogdal et al.'s (2017) model, whose visually assessed fitting for dl-PCBs in suckler calves showed deviations of up to 30% from observed means, BeefPOP achieved lower mean deviations of 16% and 20% for EXP (optimization) and DEC/CTL (evaluation) treatment datasets, respectively. Puttrevu et al. (2020) proposed a 2-fold deviation from observed values as an acceptable threshold for PBTK model predictions. Accordingly, the BeefPOP model demonstrated satisfactory predictive performance, with deviations from observations remaining below 1.4-fold for all PCB congeners and their sums. This contrasts with the model developed by Minnema et al. (2025), which showed deviations of up to 2.4-fold for

PCDD/F + dl-PCB WHO-TEQ sum in muscle lipids of bulls and cows. For ndl-PCBs, the deviations observed with the BeefPOP model were comparable to those reported by Moenning et al. (2023c) in calf blood lipids.

At both the optimization and evaluation steps, the BeefPOP model showed strong goodness of fit, with R^2 ranging from 0.79 to 0.99, and RMSE below the standard deviation of the observed mean. The accuracy was also satisfactory, with the absolute MB below 25% of the observed mean and the MAPE below 20%. These performances are comparable to those reported by Lerch et al. (2025) for the RuMoPOP lactating cow model that predicts milk PCB concentrations. The authors presented R^2 above 0.87, RMSE below the standard deviation of the observed mean, and MAPE below 20% for ndl-PCB sum and dl-PCB WHO-TEQ sum at the optimization step, as well as for PCB 126 and 169 (most important contributors to the WHO-TEQ sum) at the evaluation step. While the RRMSE was above the threshold of 50% for dl-PCB, this metric may overestimate predictive discrepancy due to a low mean concentration. Complementary metrics, including MAPE, absolute MB relative to the observed mean, and visual appreciation of kinetics, were also considered when evaluating model adequacy. Overall, these combined metrics indicate that the model reliably captures fairly the main PCB accumulation and depuration trends, supporting its satisfactory predictive performances.

When the model's evaluation was extended to muscles and the liver, its goodness of fit varied depending on the PCB congeners and treatments (e.g., R^2 values below 0.5 for ndl-PCBs for the EXP treatment). This discrepancy may be partly explained by the adjustment of partition coefficients (P_i) and ARs in the model using the experimental observations of the EXP calves at 288 days old, reflecting near steady-state conditions. By contrast, evaluation of the model's adequacy for predicting liver and muscle PCB concentrations also included data from calves that died prematurely (90 days old) when tissue distribution was still dynamic. Consequently, parameters fitted under nearly steady-state conditions may not have accurately captured early-stage dynamics. This was especially evident for PCB 28, 52, and 101. Observed concentrations in muscle at 90 days old were 10 to 20-fold higher than predicted values, while liver concentrations were overestimated by the model. These findings may also be linked to the specific physicochemical properties and metabolic susceptibility of these congeners, which present lower lipophilicity (K_{ow}), and higher k_{met}, than highly chlorinated congeners. Moreover, the model relies on a lipid-driven representation of PCB distribution and does not explicitly account for binding to tissue proteins. However, PCBs may also bind to proteins in the liver and muscles (Inui et al., 2014; Grimm et al., 2015). Such binding processes are not represented in the model, where tissue distribution is driven by lipid partitioning. The correction factors for the tissue partition *Corr* P_i are intended to account for PCB tissue distribution not fully captured by the lipid-driven partitioning. Nevertheless, the ability of the model to accurately represent PCB kinetic in protein-rich tissues may be limited, which is particularly relevant for the liver, where high *Corr* P_i values were required, as noticed by Driesen et al. (2022b).

At the early calf developmental stage of 90 days old, PCB hepatic clearance may be less efficient due to an immature liver metabolic enzyme system, as observed by Driesen et al. (2022b). This could lead to lower protein binding (the initial step of PCB metabolization) and a further lower concentration in the liver than predicted by the model, which uses a static blood-to-liver partition coefficient (P_{liver}). Consequently, less PCB elimination would occur due to hepatic clearance, leading to greater accumulation and higher concentrations in muscles. However, this observation was not clear for adipose tissues. This could be due to the use of the observed adipose tissue concentrations for k_{met} optimization purpose, and the tissue's slower perfusion and permeability-limited transfer between blood and adipose tissues that delayed the kinetic response (Richter and McLachlan, 2001; MacLachlan, 2009). Altogether, the model captured adipose tissue kinetics satisfactorily, which is important for PBTK model reliability, as adipose tissues act as the main long-term storage compartment within the body. However, limitations appeared when extrapolating to more dynamic tissues, such as the liver and muscles. Consequently, static partition coefficients do not necessarily account for body distribution kinetics early in life and are far from the steady state assumption.

4.2. Model simulations to decipher the interplay between beef cattle feeding and physiology, and PCB source of exposure

4.2.1. Effect of PCB source of exposure on accumulation kinetics

Beef cattle can be exposed to PCBs through punctual and diffusive sources, characterized by a distinct congener pattern (Malisch, 2017; Hoogenboom et al., 2020). In the present modeling investigation, three realistic exposure sources with contrasting PCB congener patterns were investigated through simulations: *Paint* (Bogdal et al., 2017), *Feed* (Heres et al., 2010), and *Soil* (Fournier et al., 2013). The sources of exposure applied in these prospective simulations were based on real case studies and are not intended to be representative of all possible contamination sources and incidents encountered in practice. In particular, the *Paint* exposure scenario derived from Bogdal et al. (2017) represents a specific contamination case of barn wall paint in a beef farm of the Grisons canton of Switzerland. The several old paint materials in use up to the 80′s, present a wide diversity of PCB congener patterns depending on pigments composition or manufacturing processes (Hu and Hornbuckle, 2010), which are not fully represented in the selected scenario.

The *Paint* source of exposure showed the most distinct PCB congener pattern when compared to *Feed* and *Soil*, which were closer, particularly in terms of the dl-PCB pattern in the WHO-TEQ sum. For *Soil* exposure, the PCB pattern corresponds to that of Fournier et al.'s (2013) study, in which goats were fed corn silage harvested in an area where soil has been contaminated by PCBs after wood fire on a polluted industrial site. The congener distribution was consistent with those reported in forage and soil samples from other contaminated areas due to waste incineration, such as Gilly-sur-Isère, France (Costera et al., 2006), the Canton of Lucerne, Switzerland (Bogdal et al., 2017), and the Campania region, Italy (Lambiase et al., 2022).

Despite equal concentrations of dl-PCB sum in the total diet across all exposure scenarios (0.40 ng TEQ.kg^{-1} DM), accumulation kinetics in growing cattle differed depending on the contamination source. The *Paint* scenario led to the highest tissue concentrations of dl-PCBs, which, on average, were 1.1- and 1.2-fold higher than the *Feed* and *Soil* exposure scenarios, respectively. This is reflected in the different BCF and AE values for dl-PCBs, which followed the same order of *Paint* > *Feed* > *Soil*, whereas for ndl-PCBs, the trend was *Soil* > *Paint* > *Feed*. These differences highlight the effect of the congener-specific profile of the source of exposure on bioaccumulation behavior. As previously suggested by Travis and Arms (1988), and reported by Amutova et al. (2021) and Driesen et al. (2021), the physicochemical properties of contaminants (i.e., lipophilicity and chlorination degree) influence transfer factors such as BCFs and AEs. Unlike PCB 126, congeners 118 and 156 are not metabolized ($k_{met} = 0$), which may explain their slightly higher accumulation in adipose tissue compared to their proportions in the diet, especially under *Paint* exposure. Overall, the dl-PCB TEQ pattern in the diet was in close agreement with patterns in adipose tissues of growing cattle, supporting the idea that the PCB congener profile in contaminated meat could enable the identification of the contamination source, as suggested by Hoogenboom et al. (2020).

For ndl-PCBs, the major contributors were PCB 138, 153, and 180 in adipose tissues, with a higher contribution of PCB 153 compared to the diet. This observation was also seen in the meat and fat of pigs fed contaminated crumbs, corresponding to the *Feed* scenario (Heres et al., 2010). Conversely, ndl-PCB 28, 52, and 101 were found at low levels in adipose tissues compared to the diet, likely due to their high metabolism rate (i.e., high k_{met}). Although the congener profiles were less variable across exposure types, the total intake differed: 104, 15.5, and 1.0 μg.kg^{-1} DM in the total intake for *Paint*, *Feed*, and *Soil* exposure,

respectively. This intake gradient led to higher ndl-PCB concentrations in the adipose tissues of animals exposed to *Paint*.

Overall, these findings indicate that the BeefPOP model is able to represent fairly divergent bioaccumulation rates at the dl-PCB and ndl-PCB sum levels, which are influenced by the physicochemical properties and metabolic susceptibility of the dominant congeners and further depend on the specific source of exposure. This underlines how hazardous it is to address PCB contamination risks in livestock production systems based on empiric factors or model simulations set at the sum level only, without considering the specific congener pattern. In addition, an intake set at the AL for dl-PCBs WHO-TEQ sum in feed (EU regulation No 277/2012) led to systematic exceedance of the ML in adipose tissue and muscle (EU regulation No 1259/2011), and liver (EU regulation No 1067/2013) under a constant exposure scenario. This highlights that compliance with AL in feed does not guarantee PCB levels below the ML in animal-derived food products. A similar finding was reported by Ohlhoff et al. (2021), who showed that the ndl-PCB concentration in feed below ML would not consistently result in chicken meat below the ML for meat.

4.2.2. *Effect of growing cattle physiology on PCB accumulation kinetics*

The BeefPOP model simulations allowed the exploration of the effects of physiological traits of cattle, depending on their category and growth itinerary, on the body accumulation of PCBs. The influence of growth physiology on POP concentrations in animal tissues was reported in previous in vivo studies (Driesen et al., 2021, 2022a for beef cattle; Krause et al., 2023 for dairy cows; Rey-Cadilhac et al., 2020; Lerch et al., 2024 for ewes). The range of feed-to-adipose tissue BCFs modeled in this study was consistent with those previously recorded in vivo for growing beef cattle (Driesen et al., 2021). Similarly, AEs were within the same range as those reported by Driesen et al. (2022b) for exposed calves aged 10 months. However, the Charolais bulls presented a higher PCB accumulation rate compared to Angus × Hereford steers, reflected by higher BCFs and tissue concentrations. This difference appears to be driven by carcass lipid content. Angus × Hereford, an early-maturing breed, had a carcass lipid content on average 1.8-fold higher than Charolais. Such increased lipid mass in the former provides higher dilution potential for PCBs, as suggested by Fernandes et al. (2011). A similar dilution effect has also been reported for PCB in growing bulls (Driesen et al., 2021) and calves (Driesen et al., 2022a). Regarding the effect of growth rate, tissue PCB concentrations, BCFs and AEs were higher in SG than in FG and CG. This effect of growth intensity is mainly explained by differences in the time required to reach the targeted BW. Lower lipid mass early in the SG itinerary, coupled with longer time to reach the BW of 700 kg, would lead to a higher cumulative PCB exposure, a lower dilution effect, and higher PCB concentrations and accumulation rates (BCFs) in the tissues. In contrast, FG itinerary allowed a shorter exposure time (i.e., slaughter occurred at a younger age when compared to SG) due to faster gains, leading to lower cumulative PCB exposure and more effective dilution, and subsequently lower PCB concentrations and BCFs in tissues. The CG itinerary showed intermediate body tissue concentrations, with a noticeable decline after the diet was switched to that of the FG treatment. Overall, increased body lipid deposition rate, whether by animal category or growth intensity, promotes contaminant dilution. This further resulted in lower PCB concentrations and BCFs in adipose tissues compared to muscles where lipid deposition, and thus dilution, occurs more slowly and later along with growth (Lerch et al., 2020, Driesen et al., 2022b). In addition, adipose tissues comprise a deep sub-compartment, characterized by permeability-limited transfer kinetics, compared to muscles. These findings underline the importance of considering both animal category-specific physiology and growth dynamics when assessing the risk of lipophilic contaminant accumulation in cattle on a case-by-case basis.

4.2.3. *PCB depuration kinetics*

During depuration, the PCB concentrations and half-lives varied between adipose tissues and muscles, highlighting tissue-specific depuration dynamics, as also reported in vivo by Driesen et al. (2022b). According to our model simulations, depuration in growing cattle depends on both the source of initial PCB exposure and cattle's physiological traits. The dl-PCB depuration half-lives were longer in the *Paint* exposure scenarios. Conversely, for ndl-PCBs, longer half-lives were observed in the *Soil* exposure scenario. These longer half-lives are consistent with higher BCFs and AEs observed during the accumulation phase, likely due to the congener-specific profile of these contamination sources, with a higher contribution of non-metabolized and more persistent PCBs (*e.g.*, dl-PCB 118 and 156 in *Paint*, and ndl-PCB 153 in *Soil*).

The SG itinerary showed longer PCB depuration half-lives compared to the FG and CG itineraries. However, even if slower in the SG itinerary, the steady deposition of lipids provided a dilution effect that, in some scenarios, allowed dl-PCB concentrations to decrease below the ML at the time of slaughter. During depuration, PCB half-lives are influenced not only by metabolism and fecal excretion, but also by growth and physiological changes. Cattle continue to gain BW while depurating, and accordingly body lipid deposition dilutes PCB concentrations in tissues. Therefore, depuration half-lives estimated by the model should be interpreted as effective rates integrating both elimination and growth dilution. This is particularly relevant for the FG itinerary, where faster lipid accretion accelerates PCB dilution effect, resulting in shorter half-lives and dl-PCB concentrations consistently decreasing below the ML in all scenarios, when compared to the SG itinerary. In accordance, the CG itinerary presented shorter dl-PCB depuration half-lives due to the fastest lipid deposition after the refeeding, increasing PCB dilution. Given that CG cattle reached slaughter weight faster than SG cattle, the time span for depuration via metabolism and fecal excretion was reduced. Altogether, the final tissue PCB levels in CG and SG cattle were similar, suggesting that compensatory growth may be a promising strategy to reduce the overall fattening period to reach specific PCB levels in meat at the end of the depuration phase. This could be particularly relevant for managing contaminated herds, as it may help reach concentrations below the ML more rapidly.

From a food safety risk assessment perspective, the BeefPOP model provides a quantitative approach to relate PCB exposure scenarios in cattle to compliance with MLs. By integrating exposure duration, growth dynamics, and depuration phases, BeefPOP can be used to explore the effectiveness of withdrawal periods and to support decisions regarding slaughter timing following a contamination event. Such applications are relevant for mitigating public health and economic risks in beef production systems.

5. Conclusion

This study demonstrated the ability of the mechanistic BeefPOP model to simulate PCB accumulation and depuration kinetics in growing cattle. Optimization and preliminary evaluation against experimental data showed very satisfactory predictive performances for individual PCB congeners and their sums in adipose tissues with a satisfactory goodness of fit. Although the predictions for muscles and the liver were slightly more variable, the model still offered valuable insights into tissue-specific kinetics. Model application to prospective scenarios revealed that PCB accumulation and depuration in fattening cattle were influenced by the source of contamination, with divergent PCB congener patterns of contrasted lipophilicity and metabolic susceptibility. A punctual source of exposure from contaminated wall paint can lead to higher dl-PCB concentrations in tissues due to the high contribution of non-metabolized congeners, whereas a dl-PCB profile from *Soil* exposure would result in lower tissue concentrations.

Furthermore, the findings show that the animal category (breed and sex and concomitant maturity degree and body fatness) and the growth intensity and itinerary substantially influence PCB kinetics. Early-maturing cattle such as Angus × Hereford steers, characterized by

high lipid deposition and faster growth, exhibited lower accumulation, due to reduced raising time and a higher PCB dilution in the body lipid mass, leading to lower PCB tissue concentrations and BCFs. Similarly, the growth rate had an effect on the toxicokinetic, with fast growth rate showing, for example, a lower accumulation rate and better depuration efficiency through reduced exposure time and faster body lipid accretion and dilution of PCBs.

Overall, this study underscores the importance of integrating contaminant properties, animal feeding and physiology, and farming practices when assessing the risk of contamination with PCBs in livestock. By coupling fugacity and PBTK concepts with growth function mechanistic modeling, the mechanistic BeefPOP model provides a valuable, generic, and adaptable tool to assess the complex interplay between contaminant source of exposure, ADME, and beef physiology on lipophilic contaminant accumulation and depuration kinetics. This integrative approach enhances risk assessment capabilities and supports management strategies to mitigate contaminant transfer from feed to food of animal origin. Furthermore, the model's structure makes it suitable for adaptation to other lipophilic contaminants (e.g., non-regulated PCB congeners, PCDD/Fs), contributing to broader food safety advances. Finally, to facilitate the use of the model for risk assessment and management, the ultimate goal is to make BeefPOP available through the ConTrans web platform (https://contrans.bfr.bund.de/), hosted by the Federal Institute for Risk Assessment (Bundesinstitut für Risikobewertung, Berlin, Germany).

Declaration of generative AI and AI-assisted technologies in the writing process

The authors did not use AI-assisted technologies for the writing of the work.

CRediT authorship contribution statement

Audrey Tiercin: Writing – review & editing, Writing – original draft, Visualization, Validation, Software, Investigation, Formal analysis. **John Albechaalany:** Writing – review & editing, Software, Methodology, Investigation, Formal analysis, Conceptualization. **Charlotte Driesen:** Writing – review & editing, Data curation. **Philippe Schmidely:** Writing – review & editing. **Isabelle Ortigues-Marty:** Writing – review & editing, Conceptualization. **Markus Zennegg:** Writing – review & editing, Resources, Data curation. **Daniel Sauvant:** Validation, Supervision, Methodology, Conceptualization. **Christelle Loncke:** Writing – review & editing, Validation, Supervision, Methodology, Conceptualization. **Sylvain Lerch:** Writing – review & editing, Writing – original draft, Visualization, Validation, Supervision, Software, Project administration, Methodology, Investigation, Funding acquisition, Formal analysis, Conceptualization.

Funding

Sylvain Lerch and Markus Zennegg acknowledge the financial support of the Federal Office for the Environment (Bern, Switzerland) under contract n°17.0082.PJ "MeatPOP: POP transfer from the feed and soil to the Swiss beef meat", the Federal Office for Agriculture (Bern, Switzerland) under contract "Improved bovine meat safety regarding organic pollutants: a modeling approach for on-farm risk assessment", and the association Mutterkuh Schweiz (Lupfig, Switzerland).

Declaration of competing interest

The authors declare that they have no known competing financial interests or personal relationships that could have appeared to influence the work reported in this paper.

Acknowledgments

The authors would like to warmly thank Jacques Agabriel (UMR Herbivores, INRAE, Theix, France) for his valuable inputs in the initial step of the model development. Scribendi (Chatham, Ontario, Canada) is acknowledged for its English proofreading.

Appendix A. Supplementary data

Supplementary data to this article can be found online at https://doi.org/10.1016/j.envint.2026.110193.

Data availability

The code of the model is provided online at https://doi.org/10.5281/zenodo.17600518. Data from the model simulations will be made available on request.

References

Amutova, F., Delannoy, M., Baubekova, A., Konuspayeva, G., Jurjanz, S., 2021. Transfer of persistent organic pollutants in food of animal origin – Meta-analysis of published data. Chemosphere 262, 128351. https://doi.org/10.1016/j.chemosphere.2020.128351.

Bogdal, C., Züst, S., Schmid, P., Gyalpo, T., Zeberli, A., Hungerbühler, K., Zennegg, M., 2017. Dynamic transgenerational fate of polychlorinated biphenyls and dioxins/furans in lactating cows and their offspring. Environ. Sci. Technol. 51, 10536–10545. https://doi.org/10.1021/acs.est.7b02968.

Cheng, Y.H., Lin, Y.J., You, S.H., Yang, Y.F., How, C.M., Tseng, Y.T., Chen, W.Y., Liao, C. M., 2016. Assessing exposure risks for freshwater tilapia species posed by mercury and methylmercury. Ecotoxicology 25, 1181–1193. https://doi.org/10.1007/s10646-016-1672-4.

Costera, A., Feidt, C., Marchand, P., Le Bizec, B., Rychen, G., 2006. PCDD/F and PCB transfer to milk in goats exposed to a long-term intake of contaminated hay. Chemosphere 64, 650–657. 1016/j.chemosphere.2005.10.052.

Derks, H.J.G.M., Berende, P.L.M., Olling, M., Everts, H., Liem, A.K.D., de Jong, A.P.J.M., 1994. Pharmacokinetic modeling of polychlorinated dibenzo-p-dioxins (PCDDs) and furans (PCDFs) in cows. Chemosphere 28, 711–715. https://doi.org/10.1016/0045-6535(94)90222-4.

Driesen, C., Zennegg, M., Morel, I., Hess, H.D., Nowack, B., Lerch, S., 2021. Average transfer factors are not enough: the influence of growing cattle physiology on the transfer rate of polychlorinated biphenyls from feed to adipose. Chemosphere 270, 129698. https://doi.org/10.1016/j.chemosphere.2021.129698.

Driesen, C., Lerch, S., Siegenthaler, R., Silacci, P., Hess, H.D., Nowack, B., Zennegg, M., 2022a. Accumulation and decontamination kinetics of PCBs and PCDD/Fs from grass silage and soil in a transgenerational cow-calf setting. Chemosphere 296, 133951. https://doi.org/10.1016/j.chemosphere.2022.133951.

Driesen, C., Zennegg, M., Rothacher, M., Dubois, S., Wyss, U., Nowack, B., Lerch, S., 2022b. Transgenerational mass balance and tissue distribution of PCBs and PCDD/Fs from grass silage and soil into cow-calf continuum. Chemosphere 307, 135745. https://doi.org/10.1016/j.chemosphere.2022.135745.

Erickson, M.D., Kaley, R.G., 2011. Applications of polychlorinated biphenyls. Environ. Sci. Pollut. Res. 18, 135–151. https://doi.org/10.1007/s11356-010-0392-1.

EFSA, 2014. Modern methodologies and tools for human hazard assessment of chemicals. EFSA J. 12, 3638–3725. https://doi.org/10.2903/j.efsa.2014.3638.

EFSA, 2018. Risk for animal and human health related to the presence of dioxins and dioxin-like PCBs in feed and food. EFSA J. 16. https://doi.org/10.2903/j.efsa.2018.5333.

Fernandes, A.R., Foxall, C., Lovett, A., Rose, M., Dowding, A., 2011. The assimilation of dioxins and PCBs in conventionally reared farm animals: occurrence and biotransfer factors. Chemosphere 83, 815–822. https://doi.org/10.1016/j.chemosphere.2011.02.083.

Fiedler, H., Kallenborn, R., de Boer, J., Sydnes, L.K., 2019. The stockhol convention: a tool for the global regulation of persistent organic pollutants. Chem. Int. 41 (2), 4–11. https://doi.org/10.1515/ci-2019-0202.

Fournier, A., Rychen, G., Marchand, P., Toussaint, H., Le Bizec, B., Feidt, C., 2013. Polychlorinated Biphenyl (PCB) decontamination kinetics in lactating goats (capra hircus) following a contaminated corn silage exposure. J. Agric. Food Chem. 61, 7156–7164. https://doi.org/10.1021/jf401048j.

Garcia, F., Sainz, R.D., Agabriel, J., Barioni, L.G., Oltjen, J.W., 2008. Comparative analysis of two dynamic mechanistic models of beef cattle growth. Anim. Feed Sci. Technol. 143, 220–241. https://doi.org/10.1016/j.anifeedsci.2007.05.012.

Giesy, J.P., Kannan, K., 1998. Dioxin-like and non-dioxin-like toxic effects of polychlorinated biphenyls (PCBs): implications for risk assessment. Crit. Rev. Toxicol. 28, 511–569. https://doi.org/10.1080/10408449891344263.

Grimm, F.A., Hu, D., Kania-Korwel, I., Lehmler, H.J., Ludewig, G., Hornbuckle, K.C., Duffel, M.W., Bergman, A., Robertson, L.W., 2015. Metabolism and metabolites of polychlorinated biphenyls (PCBs). Crit. Rev. Toxicol. 45 (3), 245–272. https://doi.org/10.3109/10408444.2014.999365.

Heres, L., Hoogenboom, R., Herbes, R., Traag, W., Urlings, B., 2010. Tracing and analytical results of the dioxin contamination incident in 2008 originating from the Republic of Ireland. Food Addit. Contam. Part A Chem. Anal. Control Expo. Risk Assess. 27 (12), 1733–1744. https://doi.org/10.1080/19440049.2010.522598.

Hoch, T., Agabriel, J., 2004a. A mechanistic dynamic model to estimate beef cattle growth and body composition: 1. Model description. Agr. Syst. 81, 1–15. https://doi.org/10.1016/j.agsy.2003.08.005.

Hoch, T., Agabriel, J., 2004b. A mechanistic dynamic model to estimate beef cattle growth and body composition: 2. Model evaluation. Agr. Syst. 81, 17–35. https://doi.org/10.1016/j.agsy.2003.08.006.

Hoogenboom, R., Traag, W., Fernandes, A., Rose, M., 2015. European developments following incidents with dioxins and PCBs in the food and feed chain. Food Control 50, 670–683. https://doi.org/10.1016/j.foodcont.2014.10.010.

Hoogenboom, R., Malisch, R., van Leeuwen, S.P.J., Vanderperren, H., Hove, H., Fernandes, A., Schächtele, A., Rose, M., 2020. Congener patterns of polychlorinated dibenzo-p-dioxins, dibenzofurans and biphenyls as a useful aid to source identification during a contamination incident in the food chain. Sci. Total Environ. 746, 141098. https://doi.org/10.1016/j.scitotenv.2020.141098.

Hu, D., Hornbuckle, K.C., 2010. Inadvertent polychlorinated biphenyls in commercial paint pigments. Environ. Sci. Technol. 44 (8), 2822–2827. https://doi.org/10.1021/es902413k.

INRA, Noziere, P., Sauvant, D., Delaby, L., 2018. INRA Feeding System for Ruminants. Wageningen Academic Publishers. ISBN: 978-90-8686-292-4.

Inui, H., Itoh, T., Yamamoto, K., Ikushiro, S.I., Sakaki, T., 2014. Mammalian cytochrome P450-dependent metabolism of polychlorinated dibenzo-p-dioxins and coplanar polychlorinated biphenyls. Int. J. Mol. Sci. 15 (8), 14044–14057. https://doi.org/10.3390/ijms150814044.

Jondreville, C., Cariou, R., Meda, B., Dominguez-Romero, E., Omer, E., Dervilly-Pinel, G., Le Bizec, B., Travel, A., Baeza, E., 2017. Accumulation of a-hexabromocyclododecane (alpha- HBCDD) in tissues of fast- and slow-growing broilers (*Gallus domesticus*). Chemosphere 178, 424–431. https://doi.org/10.1016/j.chemosphere.2017.03.064.

Kelly, B.C., Gobas, F.A.P.C., McLachlan, M.S., 2004. Intestinal absorption and biomagnification of organic contaminants in fish, wildlife, and humans. Environ. Toxicol. Chem. 23, 2324–2336. https://doi.org/10.1897/03-545.

Krause, T., Moenning, J.-L., Lamp, J., Maul, R., Schenkel, H., Fürst, P., Pieper, R., Numata, J., 2023. Transfer of polychlorinated dibenzo-p-dioxins and dibenzofurans (PCDD/Fs) and polychlorinated biphenyls (PCBs) from oral exposure into cow's milk - Part I: state of knowledge and uncertainties. Nutr. Res. Rev. 36, 448–470. https://doi.org/10.1017/s0954422422000178.

Klevenhusen, F., Südekum, K.-H., Breves, G., Kolrep, F., Kietzmann, M., Gerletti, P., Numata, J., Spolders, M., Pieper, R., Kowalczyk, J., 2021. Predicting the transfer of contaminants in ruminants by models - Potentials and challenges. ALTEX – Altern. Anim. Ex. 38, 398–418. https://doi.org/10.14573/altex.2007081.

Lambiase, S., Fiorito, F., Serpe, F.P., Trifuoggi, M., Gallo, P., Esposito, M., 2022. Bioaccumulation of PCDD/Fs and PCBs in free-range hens: congener fingerprints and biotransfer factors. Chemosphere 309, 136602. https://doi.org/10.1016/j.chemosphere.2022.136602.

Lautz, L.S., Oldenkamp, R., Dorne, J.L., Ragas, A.M.J., 2019. Physiologically based kinetic models for farm animals: critical review of published models and future perspectives for their use in chemical risk assessment. Toxicol. In Vitro 60, 61–70. https://doi.org/10.1016/j.tiv.2019.05.002.

Lerch, S., Rey-Cadilhac, L., Cariou, R., Faulconnier, Y., Jondreville, C., Roux, D., Dervilly-Pinel, G., Le Bizec, B., Jurjanz, S., Ferlay, A., 2020. Undernutrition combined with dietary mineral oil hastens depuration of stored dioxin and polychlorinated biphenyls in ewes. 2. Tissue distribution, mass balance and body burden. PLoS One 15. https://doi.org/10.1371/journal.pone.0230628.

Lerch, S., Siegenthaler, R., Numata, J., Moenning, J.-L., Dohme-Meier, F., Zennegg, M., 2024. Accumulation rate, depuration kinetics, and tissue distribution of polychlorinated dibenzo-p-dioxins and dibenzofurans (PCDD/Fs) in suckler ewes (Ovis aries). J. Agric. Food Chem. 72, 14941–14955. https://doi.org/10.1021/acs.jafc.4c02626.

Lerch, S., Martin, O., Fournier, A., Ortigues-Marty, I., Henri, J., 2025. Combining fugacity and physiologically based toxicokinetic concepts in a mechanistic model describing the fate of lipophilic contaminants in lactating cows. Environ. Int. 199, 109509. https://doi.org/10.1016/j.envint.2025.109509.

Li, M., Gehrin, R., Riviere, J.E., Lin, Z., 2018. Probabilistic physiologically based pharmacokinetic model for penicillin G in milk from dairy cows following intramammary or intramuscular administrations. Toxicol. Sci. 164, 85–100. https://doi.org/10.1093/toxsci/kfy067.

Mackay, D., 2001. Multimedia environmental models: the fugacity approach, second ed. CRC Press Taylor & Francis Group, Ann Arbor.

MacLachlan, D.J., 2009. Influence of physiological status on residues of lipophilic xenobiotics in livestock. Food Addit. Contam. Part A Chem. Anal. Control Expo. Risk Assess. 26, 692–712. https://doi.org/10.1080/02652030802669170.

MacLachlan, D.J., Bhula, R., 2009. Transfer of lipid-soluble pesticides from contaminated feed to livestock, and residue management. Anim. Feed Sci. and Technol. 149, 307–321. https://doi.org/10.1016/j.anifeedsci.2008.06.007.

Malisch, R., Kotz, A., 2014. Dioxins and PCBs in feed and food – Review from European perspective. Sci. Total Environ. 491–492, 2–10. https://doi.org/10.1016/j.scitotenv.2014.03.022.

Malisch, R., 2017. Incidents with dioxins and PCBs in food and feed-investigative work, risk management and economic consequences. J. of Environ. Prot. 8, 744–785. https://doi.org/10.4236/jep.2017.86048.

Martin, O., Sauvant, D., 2007. Dynamic model of the lactating dairy cow metabolism. Animal 1143–1166. https://doi.org/10.1017/s1751731107000377.

McLachlan, M.S., 1993. Mass balance of polychlorinated-biphenyls and other organochlorine compounds in a lactating cow. J. Agric. Food Chem. 41, 474–480. https://doi.org/10.1021/jf00027a024.

McLachlan, M.S., 1994. Model of the fate of hydrophobic contaminants in cows. Environ. Sci. Technol. 28, 2407–2414.

Méda, B., Travel, A., Guyot, Y., Henri, J., Royer, E., Baéza-Campone, E., Jondreville, C., 2020. A PBPK model to study the transfer of α-hexabromocyclododecane (α-HBCDD) to tissues of fast- and slow-growing broilers. Food Addit. Contam. Part A Chem. Anal. Control Expo. Risk Assess. 37, 316–331. https://doi.org/10.1080/19440049.2019.1681596.

Mi, K., Lin, Z., 2025. Chemical risk assessment in food animals via physiologically based pharmacokinetic modeling – Part II: environmental pollutants on animal and human health assessments. Environ. Int. 198, 109372. https://doi.org/10.1016/j.envint.2025.109372.

Minnema, J., Notenboom, S., Westerhout, J., Hoogenboom, R., Jeurissen, S., 2025. Congener-specific transfer modelling of dioxins and dioxin-like PCBs in free-ranging cattle grazing in the dutch floodplains. Food Addit. Contam. Part A Chem. Anal. Control Expo. Risk Assess. 42 (5), 603–620. https://doi.org/10.1080/19440049.2025.2478076.

Moenning, J.-L., Krause, T., Lamp, J., Maul, R., Schenkel, H., Fürst, P., Pieper, R., Numata, J., 2023a. Transfer of polychlorinated dibenzo-p-dioxins and dibenzofurans (PCDD/Fs) and polychlorinated biphenyls (PCBs) from oral exposure into cow's milk - Part II: Toxicokinetic predictive models for risk assessment. Nutr. Res. Rev. 36 (2), 484–497. https://doi.org/10.1017/s0954422422000208.

Moenning, J.-L., Lamp, J., Knappstein, K., Molkentin, J., Susenbeth, A., Schwind, K.-H., Dänicke, S., Fürst, P., Schenkel, H., Pieper, R., Krause, T., Numata, J., 2023b. Toxicokinetic modeling of the transfer of polychlorinated biphenyls (PCBs) and polychlorinated dibenzo-p-dioxins and dibenzofurans (PCDD/Fs) into milk of high-yielding cows during negative and positive energy balance. Comput. Toxicol. 28, 100290. https://doi.org/10.1016/j.comtox.2023.100290.

Moenning, J.-L., Numata, J., Bloch, D., Jahnke, A., Schafft, H.A., Spolders, M., Lüth, A., Lahrssen-Wiederholt, M., Schulz, K., 2023c. Transfer and toxicokinetic modeling of non-dioxin-like polychlorinated biphenyls (ndl-PCBs) into accidentally exposed dairy cattle and their calves - a case report. Environ. Toxicol. Pharmacol. 99, 104106. https://doi.org/10.1016/j.etap.2023.104106.

Ohlhoff, B., Savvateeva, D., Bernsmann, T., Spolders, M., Jahnke, A., Lüth, A., Lahrssen-Wiederholt, M., Numata, J., Pieper, R., 2021. Unraveling congener-specific transfer of non-dioxin-like polychlorinated biphenyls (ndl-PCBs) from feed into chicken meat. Environ. Sci. Technol. 55, 11080–11090. https://doi.org/10.1021/acs.est.1c02650.

Pajurek, M., Warenik-Bany, M., Mikolajczyk, S., 2022. Feed as a source of dioxins and PCBs. Chemosphere 308, 136243. https://doi.org/10.1016/j.chemosphere.2022.136243.

Puttrevu, S.K., Arora, S., Polak, S., Patel, N.K., 2020. Physiologically based pharmacokinetic modeling of transdermal selegiline and its metabolites for the evaluation of disposition differences between healthy and special populations. Pharmaceutics 12, 942. https://doi.org/10.3390/pharmaceutics12100942.

Rey-Cadilhac, L., Cariou, R., Ferlay, A., Jondreville, C., Delavaud, C., Faulconnier, Y., Alcouffe, S., Faure, P., Marchand, P., Le Bizec, B., Jurjanz, S., Lerch, S., 2020. Undernutrition combined with dietary mineral oil hastens depuration of stored dioxin and polychlorinated biphenyls in ewes. 1. Kinetics in blood, adipose tissue and faeces. PlosOne 15, e0230629. https://doi.org/10.1371/journal.pone.0230629.

Richter, W., McLachlan, M.S., 2001. Uptake and transfer of PCDD/Fs by cattle fed naturally contaminated feedstuffs and feed contaminated as a result of sewage sludge application. 2. Nonlactating cows. J. Agric. Food Chem. 49, 5857–5865. https://doi.org/10.1021/jf010859f.

Robelin, J., 1986. Composition corporelle des bovins: Evolution au cours du développement et différences entre races [Body composition of cattle: Evolution during development and differences between breeds]. Université De Clermont-Ferrand II, 391.

Rosenbaum, R.K., McKone, T.E., Jolliet, O., 2009. CKow: a dynamic model for chemical transfer to meat and milk. Environ. Sci. Technol. 43, 8191–8198. https://doi.org/10.1021/es803644z.

Sewell, F., Alexander-White, C., Brescia, S., Currie, R.A., Roberts, R., Roper, C., Vickers, C., Westmoreland, C., Kimber, I., 2024. New approach methodologies (NAMs): Identifying and overcoming hurdles to accelerated adoption. Toxicol. Res. 13, tfae044. https://doi.org/10.1093/toxres/tfae044.

Takaki, K., Wade, A.J., Collins, C.D., 2015. Assessment and improvement of biotransfer models to cow's milk and beef used in exposure assessment tools for organic pollutants. Chemosphere 138, 390–397. https://doi.org/10.1016/j.chemosphere.2015.04.032.

Tedeschi, L.O., 2006. Assessment of the adequacy of mathematical models. Agr. Syst. 89, 225–247. https://doi.org/10.1016/j.agsy.2005.11.004.

Thomas, G.O., Sweetman, A.J., Jones, K.C., 1999. Input-output balance of polychlorinated biphenyls in a long-term study of lactating dairy cows. Environ. Sci. Technol. 33, 104–112. https://doi.org/10.1021/es980322r.

Travis, C.C., Arms, A.D., 1988. Bioconcentration of organics in beef, milk, and vegetation. Environ. Sci. Technol. 22, 271–274. https://doi.org/10.1021/es00168a005.

Van den Berg, M., Birnbaum, L.S., Denison, M., De Vito, M., Farland, W., Feeley, M., Fiedler, H., Hakansson, H., Hanberg, A., Haws, L., Rose, M., Safe, S., Schrenk, D., Tohyama, C., Tritscher, A., Tuomisto, J., Tysklind, M., Walker, N., Peterson, R.E., 2006. The 2005 World Health Organization reevaluation of human and mammalian toxic equivalency factors for dioxins and dioxin-like compounds. J. Toxicol. Sci. 93, 223–241. https://doi.org/10.1093/toxsci/kfl055.

Weber, R., Herold, C., Hollert, H., Kamphues, J., Ungemach, L., Blepp, M., Ballschmiter, K., 2018a. Life cycle of PCBs and contamination of the environment and of food products from animal origin. Environ. Sci. Pollut. Res. Int. 25, 16325–16343. https://doi.org/10.1007/s11356-018-1811-y.

Weber, R., Herold, C., Hollert, H., Kamphues, J., Blepp, M., Ballschmiter, K., 2018b. Reviewing the relevance of dioxin and PCB sources for food from animal origin and the need for their inventory, control and management. Environ. Sci. Eur. 30, 42. https://doi.org/10.1186/s12302-018-0166-9.

Xavier, C., Driesen, C., Siegenthaler, R., Dohme-Meier, F., Le, C.Y., Lerch, S., 2022. Estimation of empty body and carcass chemical composition of lactating and growing cattle: comparison of imaging, adipose cellularity, and rib dissection methods. Transl. Anim. Sci. 6, 1–14. https://doi.org/10.1093/tas/txac066.

Zennegg, M., 2018. Dioxins and PCBs in meat – still a matter of concern? Chimia 72, 690. https://doi.org/10.2533/chimia.2018.690.